

TOPICAL REVIEW • OPEN ACCESS

Terahertz MEMS metadevices

To cite this article: Prakash Pitchappa *et al* 2021 *J. Micromech. Microeng.* **31** 113001

View the [article online](#) for updates and enhancements.



The Electrochemical Society
Advancing solid state & electrochemical science & technology
2021 Virtual Education

Intensive Short Courses

Sunday, October 10 & Monday, October 11





Providing students and professionals with in-depth education on a wide range of topics

[CLICK HERE TO REGISTER](#)



Topical Review

Terahertz MEMS metadevices

Prakash Pitchappa¹ , Abhishek Kumar^{2,3}, Ranjan Singh^{2,3} , Chengkuo Lee⁴ 
and Nan Wang^{1,*} 

¹ Institute of Microelectronics, Agency for Science, Technology and Research, Singapore, Singapore

² Department of Physics and Applied Physics, Nanyang Technological University, Singapore, Singapore

³ Center for Disruptive Photonic Technologies, Nanyang Technological University, Singapore, Singapore

⁴ Department of Electrical and Computer Engineering, National University of Singapore, Singapore, Singapore

E-mail: wangn@ime.a-star.edu.sg

Received 24 February 2021, revised 3 June 2021

Accepted for publication 18 August 2021

Published 17 September 2021

**Abstract**

Terahertz (THz) part of the electromagnetic spectrum (0.1–10 THz) holds the key for next-generation high-speed wireless communication, non-destructive biosensing, fingerprint chemical detection and imaging for astronomy and security surveillance. The limited THz response of naturally occurring materials had left a technological gap in the THz region of the electromagnetic spectrum. Artificially engineered materials termed as ‘metamaterials’, have shown great potential in THz wave interaction and its active counterpart termed as ‘metadevices’ have been widely reported for on-demand manipulation of THz waves. One of the most efficient means of realizing metadevices is to reconfigure the shape of unit cells and hence the corresponding THz response. The 50+ years of development in microelectromechanical systems (MEMS) and the wide array of microactuator designs provide a perfect platform to achieve structural reconfiguration of microscale metamaterial unit cells in both in-plane and out-of-plane directions. In this review, we present a comprehensive overview of various MEMS approaches adopted for the demonstration of THz metadevices, their advantages and limitations. The future research directions of THz MEMS metadevices are also discussed. The seamless integration of matured MEMS technology with incipient THz metamaterials provides significant advantages in terms of enhanced performances, advanced functionalities and large scale manufacturability, that is critical for the development of future THz technologies.

Keywords: MEMS, terahertz, reconfigurable metamaterials, metadevices

(Some figures may appear in colour only in the online journal)

* Author to whom any correspondence should be addressed.



Original content from this work may be used under the terms of the [Creative Commons Attribution 4.0 licence](https://creativecommons.org/licenses/by/4.0/). Any further distribution of this work must maintain attribution to the author(s) and the title of the work, journal citation and DOI.

Nomenclature

6G	Sixth generation
CESRR	Complementary electrical split ring resonator
CMOS	Complementary metal oxide semiconductor
DC	Direct current
EIT	Electromagnetically induced transparency
ESRR	Electrical split ring resonator
EGaIn	Eutectic gallium indium
LC	Inductive-capacitive
LH	Left-handed
MEMS	Micro-electro-mechanical system
MIM	Metal-insulator-metal
NMOS	Negative-channel metal oxide semiconductor
PDMS	Polydimethylsiloxane
PEN	Polyethylene naphthalate
PET	Polyethylene terephthalate
PPy	Polypyrrole
REDOX	Reduction-oxidation
RH	Right-handed
SMA	Shape memory alloy
SRR	Split ring resonator
TE	Transverse electric
THz	Terahertz
TM	Transverse magnetic

1. Introduction to terahertz metadvicees

Terahertz (THz) region of the electromagnetic spectrum spans the frequency range of 0.1–10 THz. It is sandwiched between the electronics-dominated microwaves on the lower frequency side and the photonics-dominated infrared region on the higher frequency side. Hence, THz waves possess the combined benefits of both its neighbouring spectral regions, enabling various disruptive applications, such as high-speed wireless communication, non-destructive biological sensing, fingerprint chemical detection and imaging for astronomy and security surveillance [1–3]. However, technological development for efficient THz wave generation, detection and manipulation has remained largely limited. This is mainly due to the minimal interaction of THz waves with naturally occurring materials. Additionally, the efficient scaling up of matured microwave electronic technologies to high frequency THz or scaling down of infrared photonic technologies to low photon energy THz has been challenging. This has led to a technological gap in THz part of the electromagnetic spectrum. However, the demand for high data rate wireless communication links, highly sensitive biosensing and non-destructive imaging has accelerated the development of electronics, photonics as well as hybrid solutions for enabling THz technologies, over the past decade [4–9]. Especially, the advent of metamaterials has played a crucial role in bridging the THz technological gap. Metamaterial is an array of sub-wavelength structures, whose properties are predominantly determined by the geometry of the subwavelength structures. The subwavelength structure is also known as the ‘unit cell’ or ‘meta-atom’. The unit cells can vary widely in their shapes and sizes. Thus, metamaterials are functionally versatile, spectrally scalable, easily realizable and extremely thin and lightweight. A wide

range of metamaterials have been reported for the interaction and manipulation of various aspects of THz waves, including amplitude, frequency, phase, bandwidth, polarization, absorption, chirality, resonance lineshape, and group velocity [10–21].

THz metamaterial with tunable response is termed as ‘THz metadvicee’ and is a rapidly growing research field, owing to its importance from application standpoint. A plethora of THz metadvicees have been reported over the past 15 years. THz metadvicees can be broadly categorized into two classes, based on the active element included within the unit cell geometry to provide dynamic control—(a) inclusion of active materials, whose properties can be tuned with external stimulus and (b) structural reconfiguration of unit cell geometry using microelectromechanical systems (MEMS). The myriad of active materials with wide range of properties makes it extremely attractive for the realization of THz metadvicees with varied functionalities. These active materials can be incorporated into the metamaterial as the substrate, surrounding media, part of the resonator or as an entire resonator itself. Various material systems have been explored for THz metadvicees, including conventional semiconductors [22–37], phase change materials [38–41], phase transition materials [42–48], liquid crystals [49–53], 2D materials [54–65], 3D semimetals [66], topological insulators [67], perovskites [68–74], complex oxides [75–78] and superconductors [79–89]. The properties of these materials can be actively controlled with external stimuli such as electrical, optical, thermal or magnetic field. Even though, active material inclusion has been the most popular choice for realizing THz metadvicees, the incorporation of additional materials brings in complication with respect to limited performance, fabrication complexity, and system level integration. Alternatively, structurally reconfigurable THz metadvicees are realized through the integration of MEMS microactuators within the microscale unit cell geometry of THz metamaterials. MEMS technology has been developed for over 50 years and has widespread applications involving miniaturized, high-performance sensing and micro/nanoscale actuation [90–92]. The microscale dimension of MEMS actuators perfectly complements the micron-sized THz metamaterial unit cells. Hence, MEMS provides an ideal platform for the development of integrated THz metadvicees [93]. Reviews on MEMS for reconfigurable metamaterials operating across the wide spectral range have been reported [94–98]. Alternatively, review on integration of MEMS for THz technologies including sources, detectors and functional components have also been recently reported [99, 100]. Here, we provide a comprehensive review with focus on MEMS actuator designs that have been exclusively reported for THz metadvicees. Such focused review is important as the research efforts on developing metamaterial based solutions have started to gain significant research momentum, primarily propelled by THz-centric 6G communication [101], THz based viral sensing [102] and bioimaging. More specifically, MEMS metadvicees will play an important role in the development of reconfigurable intelligent surfaces [103–105], holographic beam formers [35], phased array antennas [106], and lens-less THz systems [107].

2. MEMS for THz metadevices

MEMS technology has enabled a wide variety of microactuators with varied performance in terms of deformation range, reconfiguration direction, response time, power consumption, ease of integration and CMOS compatibility. Various types of microstructures can be realized with MEMS, including cantilevers, beams, diaphragms and frames. These microstructures can be mechanically deformed with external applied fields and are known as 'microactuators'. Microactuators integrated with metamaterial unit cells enable dynamic reshaping of unit cell geometries, thereby providing tunable THz response. Various designs of microstructures adopted for THz MEMS metadevices are elaborated next. Cantilever is the simplest of microstructures that is fixed at one end and free to move at the other end. Upon applying force, maximum displacement will be achieved at the free end of the cantilever. Beams are similar to cantilevers, but are fixed at both ends. Upon applying force, maximum deformation occurs at the midpoint of the beam. Diaphragms are membrane-like structures, which are fixed on the entire perimeter and maximum deformation is observed at the centre point of the membrane. The anchors and actuation regions in these microactuators are amalgamated and hence the deformation of the microstructures are non-uniform. To achieve uniform deformation, membranes with isolated anchors are widely used. All of the aforementioned microstructures are usually adopted for out-of-plane reconfiguration of the unit cell geometry. Alternatively, frames have been adopted for inplane reconfiguration of unit cell geometry by attaching with external actuators. Frame is a slab of material with an array of perforated holes, and are usually made of silicon (Si). The frame houses a part of the unit cells and is connected to external actuators, while the other part of the unit cell is fabricated on fixed Si structures. The in-plane movable actuators drive the frame along with a part of unit cell, relative to the fixed part of unit cell to provide dynamic THz response. Various actuation mechanisms such as thermal, electrostatics, piezoelectrics, and electromagnetics can be utilized for driving the aforementioned microstructures. Among these approaches, thermal and electrostatic schemes are widely adopted, owing to their large deformation range and ease of integration. Experimental demonstrations using piezoelectric and electromagnetic approaches are yet to be reported, owing to their integration complexity. Beyond these four actuation schemes, pneumatics approach is reported for large and bi-directional reconfiguration, which is critical for specific application such as chirality switching. Furthermore, electroactive polymers which expand and contract upon applying voltage have also been reported for in-plane reconfigurable THz MEMS metadevices. Alternatively, metamaterials fabricated on flexible and stretchable substrates provide a straightforward means of achieving structural reconfiguration through mechanical bending or strain and have been reported for THz MEMS metadevices. Microfluidics integrated THz metadevices that can be filled with controlled portions of liquid metals have also been reported for THz MEMS metadevices. In this review, the reported literatures on THz MEMS metadevices are categorized

based on the reconfiguration schemes. Each reconfiguration scheme is further sub-divided based on the actuator designs to highlight the advantages, limitations and functionalities enabled by specific microactuator design. The review concludes with the future prospects of THz MEMS metadevices in terms of novel explorations and potentially disruptive applications.

2.1. Thermal reconfiguration

Thermally reconfigurable microactuators are one of the popular class of MEMS actuators, which provide microscale mechanical deformation in response to change in temperature. The thermal stimulus can be provided using a furnace, heater stage or Joule's heating by passing current. Various designs of thermal actuators for both in-plane and out-of-plane reconfiguration are available [108]. Thermal actuators provide large deformation, large stroke, continuous tunability and are relatively simpler to design and fabricate. However, thermal actuators are usually limited by their slower speed, higher power consumption, global control, sensitivity to temperature and pressure variations. Various thermally reconfigurable THz MEMS metadevices have been explored and are presented in this section.

2.1.1. Out-of-plane thermal reconfiguration. One of the initial demonstration of THz MEMS metadvice was reported using thermally reconfigurable bimaterial cantilevers. The metamaterial unit cell comprised of gold (Au) split ring resonator (SRR) on silicon nitride (SiN) membrane as shown in figure 1(a) [109]. The silicon (Si) substrate underneath the unit cell was completely etched away, leaving the SiN membrane suspended with two cantilever anchors, attached to the substrate. The cantilevers were made of bimaterial stack of Au/SiN layers. Upon fabrication, the released SiN membranes housing the Au SRRs remained relatively flat as shown in figure 1(b). Rapid thermal annealing was used to anneal the fabricated metadvice from 350 °C to 550 °C, in steps of 50 °C. After each annealing step, the bimaterial cantilevers were permanently curved up with a larger deformation as shown in figure 1(c). The released membranes housing the SRRs were lifted from ~0° (flat) after fabrication to ~65° (almost upright position) after annealing at 550 °C. This resulted in a large change in the THz response of the metadvice after each annealing step for both E_x and E_y incidence of THz waves as shown in figures 1(d) and (e), respectively. Hence, by incorporating thermally driven bimaterial cantilevers with SRR unit cells, a large change in anisotropic THz response was demonstrated through reorientation of metadvice. This approach was also adopted to demonstrate spatially selective reconfiguration of unit cells by placing the bimaterial cantilevers on desired unit cells, while the other unit cells were placed on an anchorless SiN membrane that were non-deformable [110]. Upon annealing, only the unit cells suspended with bimaterial cantilevers were deformed and allowed for spatially selective reconfiguration of the THz MEMS metadvice. Hence, large and continuous deformation of unit cell

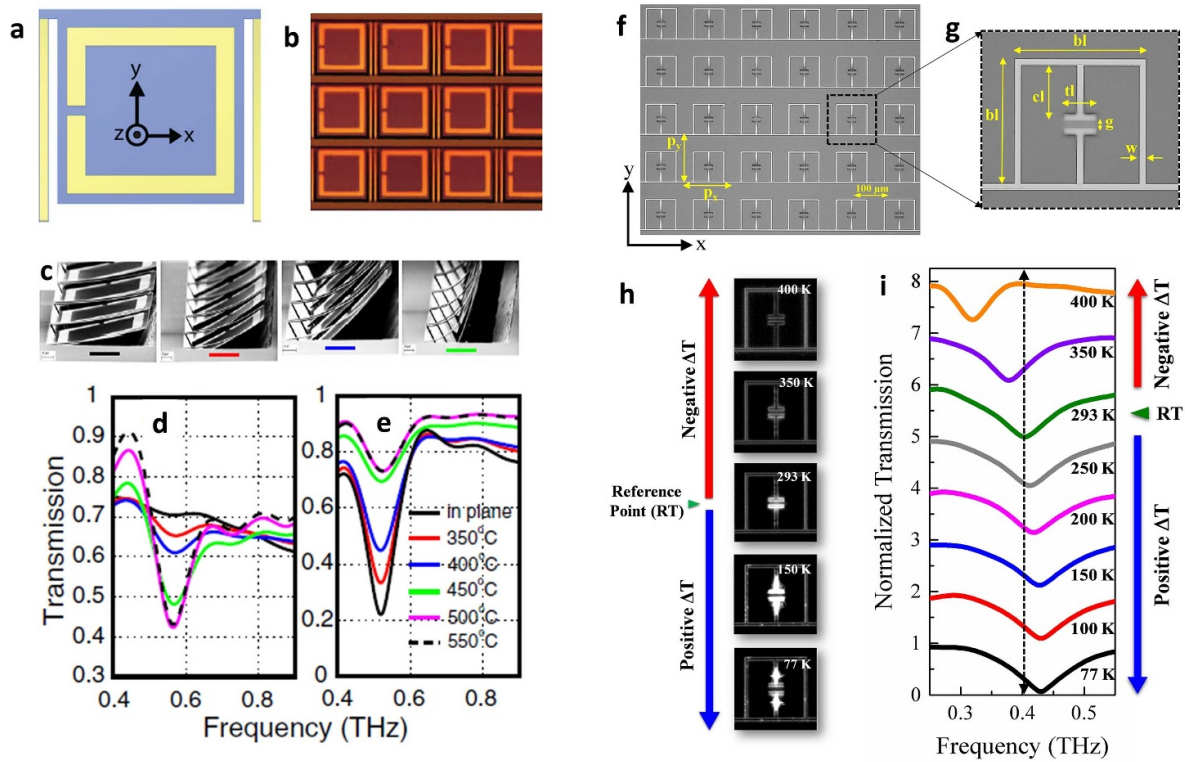


Figure 1. Thermally reconfigurable THz MEMS metadevices. (a) Schematic representation of Au SRR unit cell on SiN membrane with two bimaterial cantilevers as anchors on either side, (b) optical image (OM) of the fabricated SRR metadvice, (c) scanning electron microscope (SEM) images of the SRR metadvice before and after annealing at 350 °C, 400 °C, and 450 °C and THz transmission response of the SRR metadvice before and after annealing at different temperatures for (d) E_x incidence and (e) E_y incidence, respectively. Reprinted figure with permission from [109], Copyright (2009) by the American Physical Society. (f) OM image of the fabricated ESRR metadvice and (g) corresponding unit cell with geometrical parameter definition, (h) OM image of ESRR unit cell at different temperatures and (i) THz transmission spectra of the ESRR metadvice with decreasing and increasing temperature gradient with respect to room temperature for E_y polarization of incident THz waves. Reprinted from [111], with the permission of AIP Publishing.

geometry with spatially-selective control was demonstrated using thermal annealing of bimaterial cantilever approach. However, this mechanical reconfiguration is caused due to the changes in residual stress in the bimaterial layers forming the cantilevers and so, the deformation of the cantilever after each annealing cycle is non-volatile and cannot be reversed. This limited the operation of these metadevices to a single cycle. The proposed approach also suffers from high power consumption and requires furnace to anneal the sample at such high temperatures.

Multicycle operation of thermally reconfigurable THz MEMS meta device was also reported using bimaterial cantilevers comprising of materials with largely different coefficient of thermal expansion [111]. Temperature driven differential expansion/contraction of the constituent material layers, results in an overall out-of-plane deformation of the bimaterial cantilever. The direction of out-of-plane deformation (i.e. upwards or downwards) with increasing temperature will be determined by the relative placement of the two materials forming the cantilever. Bimaterial cantilevers made of aluminium (Al) and aluminium oxide (Al_2O_3) stack were formed as a part of electrical SRRs (ESRR) on top of Si substrate as shown in figure 1(f). Upon fabrication, the bimaterial cantilevers were deformed upwards (away from the substrate),

owing to the residual stress in the bimaterial layers as shown in figure 1(g). The measured resonance frequency of the ESRR at room temperature (300 K) was at ~ 0.4 THz as shown in figure 1(i). When the temperature of the metadvice was gradually decreased from room temperature to 77 K, the bimaterial cantilevers curved upwards as shown in figure 1(h). This led to a continuous blue-shift of the resonance frequency until 0.42 THz at 77 K, as shown in figure 1(i). Alternatively, when the temperature was gradually increased to 400 K, the cantilevers continuously curved downwards as shown in figure 1(h), leading to a red-shift in resonance frequency upto 0.32 THz as shown in figure 1(i). The THz resonance spectral tunability of ~ 0.1 THz was achieved for the overall temperature change of 323 K. Hence, a continuous, bidirectional and repeatable operation of thermally driven THz MEMS metadvice was experimentally demonstrated. Even though, multicycle operation of metadvice was demonstrated using thermal actuation, the need for external cooling and heating systems, higher power consumption and slower speed are some of the major technological challenges that needs to be addressed.

2.1.2. Electrothermal reconfiguration. Electrical current driven Joule heating of resistive elements can enable highly

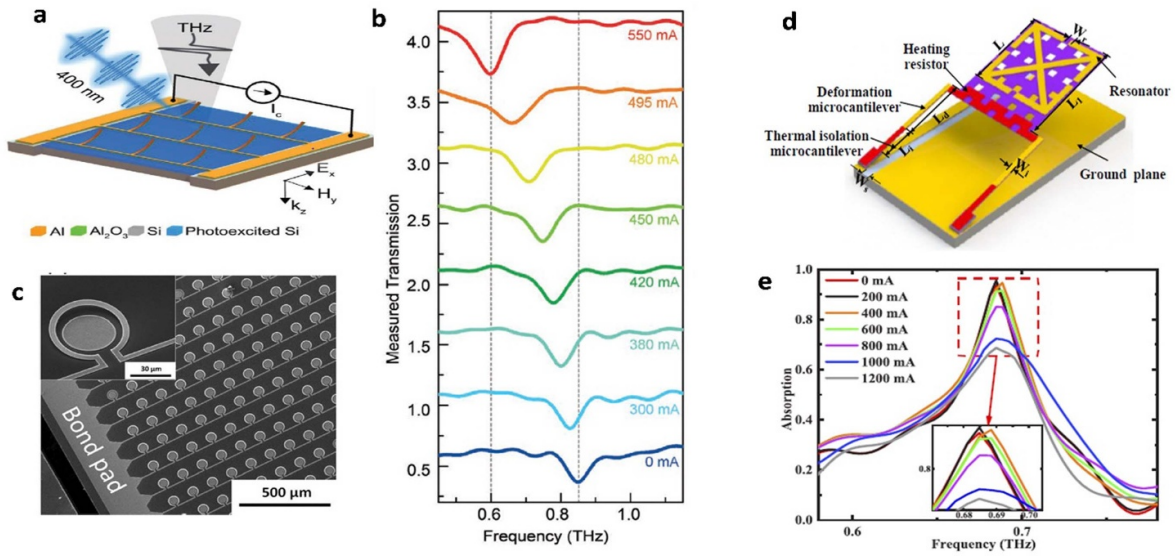


Figure 2. Electrothermally reconfigurable THz MEMS metadevices. (a) Schematic of bimaterial cantilever array as cut wire resonator metamaterial reconfigured through Joule heating with input current stimulus and (b) the measured THz transmission spectra of the cantilever metamaterial with increasing current stimulus. [112] John Wiley & Sons. [original copyright notice]. (c) SEM image of ‘Ω’-ring resonator encompassing a disk resonator was also used to demonstrate electrothermal reconfiguration of THz response. Reprinted from [113], with the permission of AIP Publishing. (d) Schematic of electrothermally reconfigurable THz metamaterial absorber and (e) measured THz absorption of the metadvice with increasing current stimulus. Reproduced with permission from [114].

compact solutions, while providing all the functional benefits of thermally reconfigurable bimaterial cantilevers. Electrically connected 2D array for bimaterial cantilevers was reported for electrothermal reconfiguration of THz resonance frequency as shown in figure 2(a) [112]. The bimaterial cantilever was made of Al and Al₂O₃ material stack and was deformed upwards upon fabrication due to residual stress. The measured resonance frequency of the as-fabricated metadvice without input current (0 mA) was at 0.85 THz as shown in figure 2(b). When electrical current was passed through the Al lines, the temperature of the entire metadvice increased due to Joule heating. This rise in temperature led to the downward deformation of cantilevers, thereby causing the resonance frequency of the metadvice to continuously red shift until 0.6 THz for 550 mA of input current as shown in figure 2(b). Similar approach was earlier adopted in a released ‘Ω’-ring enclosing a disk resonator based metadvice as shown in figure 2(c) [113].

Electrothermal actuation was also reported for active control of THz absorption [114]. Metamaterial absorbers are made of three layers—bottom reflector, dielectric spacer and top metamaterial layer. The metamaterial unit cell consisted of Au SRR on SiN plate, which was suspended by two bimaterial cantilevers made of Au/SiN with an air gap, over Au coated Si substrate which acted as the reflector, as shown in figure 2(d). The air gap between the bottom Au and top metamaterial layer formed the spacer layer. Tungsten heating resistors with thermal isolations were integrated within the unit cell to enable efficient heating of the bimaterial cantilevers. The temperature of the device was increased by passing current through the tungsten heater. With increasing temperature, the bimaterial cantilevers bent downwards, thereby reducing the air

gap between the top SRR layer and bottom Au reflector. This consequently led to a reduction in absorption at ~0.68 THz by 30% for the input current of 1200 mA as shown in figure 2(e). Hence, electrothermal approach is highly attractive for integrated solutions with large and continuous deformation. However, it still suffers from high power consumption, slower speed and high sensitivity to temperature and pressure variations.

2.1.3. In-plane thermal reconfiguration. Complementary to the out-of-plane reconfiguration, thermal actuators can also enable in-plane reconfiguration i.e. in the plane of the metamaterial. In-plane reconfigurable thermal actuators are made from single material layer. The popular choices of thermal unimorph actuator designs are the V-beam and U-beam actuators. The V-beam actuator also known as ‘chevron actuator’, is made of a long beam that is fixed on either side with a slight bend at the mid section, hence forming a V-shape [115]. When electrical current is passed through the V-beam, the Joule heating increases the temperature of the V-beam. This leads to the expansion of the V-beam and the mid section of the V-beam is pushed forward. Adoption of such in-plane reconfiguration for THz MEMS metadvice has been theoretically proposed [116]. The design proposed the use of metallic inclusion attached to the mid-portion of V-beam actuator integrated with SRR unit cells. By moving the metallic inclusion on the V-beam actuator, the effective capacitance of the SRR gap could be altered, thereby leading to a corresponding spectral tuning of SRR resonance frequency. Another popular unimorph thermal actuator for in-plane reconfiguration is the U-beam actuator and was also proposed for THz MEMS metadvice

[117]. U-beam actuator consists of two geometrically dissimilar beams connected in the shape of 'U'. Upon passing electrical current, the two beams forming the U-beam heats up by varied proportion, dictated by their respective geometrical resistance. This leads to differential expansion between the two beams. Since, the two beams are mechanically connected, an overall in-plane deformation of the U-beam is achieved. A variation of U-beam called the two-hot arm actuator was proposed for resonance frequency tuning of THz MEMS metadvice [117]. The two hot-arm actuator consists of two thin arms connected to third thicker arm. This design variation provided larger deformation for a given current stimulus. Two of these actuators with thick arm made of metal is placed with a small gap from a SRR unit cell gap. Upon applying electrical current, the metallic part of the two-hot arm actuators move toward the SRR gap and reduces the effective capacitance. This results in a continuous tuning of SRR resonance frequency. Even though, the theoretical proposals highlight the potential of in-plane reconfigurable thermal actuators for THz MEMS metadvice, there are some important fabrication-related challenges that need to be addressed for the realization of these metadvice, such as high sensitivity to stress in longer beams, inherent residual stress and temperature dependent out-of-plane deformation in bilayer beams.

2.2. Electrostatic reconfiguration

Electrostatics is arguably the most popular choice of actuation mechanism used for the demonstration of THz MEMS metadvice. Electrostatic actuator usually consists of two electrodes—one fixed and other movable with an air gap between them. When voltage is applied across the electrodes, charges of opposite polarity accumulate at the surface of the electrodes, similar to that of a capacitor. This charge accumulation leads to an attractive force between the electrodes and pulls the suspended electrode towards the fixed electrode. Electrostatic actuators provide numerous advantages, such as ease of design, smaller footprint, potentially localized control, low power consumption and simpler fabrication. On the other hand, electrostatic actuators suffer from lower deformation range, owing to pull-in phenomenon and high actuation voltages that rapidly scale up with the air gap between the electrodes. Numerous reports on electrostatically driven THz MEMS metadvice with varied functionalities are discussed in this section.

2.2.1. Out-of-plane electrostatic reconfiguration. The simplest of the electrostatic actuator is a conductive cantilever fabricated on top of a lightly doped silicon substrate with an insulating layer in between. An array of cantilevers made of Al/Al₂O₃ bimaterial stack, fabricated on top of lightly doped Si substrate was reported to provide excellent dynamic THz performance [118]. The cantilevers were prestressed due to the residual stress between the bimaterial layers and were bent upwards after the release process, as shown in figure 3(a). This allowed for a much larger tip displacement of the released cantilevers (in μm), compared to the sacrificial silicon oxide

(SiO₂) layer thickness of only 100 nm. It was also shown that by decreasing the thickness of Al layer, while keeping the Al₂O₃ thickness unchanged, resulted in an enhancement of initial tip displacement of the fabricated cantilevers. This consequently increased the tunable range of the resonance frequency of the cantilever-based THz MEMS metadvice. The dipole resonance of the cantilever metadvice for Al thickness of 100 nm, 300 nm and 500 nm were measured to be 0.88 THz, 0.935 THz and 0.96 THz, respectively as shown in figure 3(b). By applying voltage between the Al layer and Si substrate, the cantilevers were deformed towards the substrate, until it came in complete physical contact with the substrate. In this configuration, the ON state resonance for all three metadvice was ~ 0.6 THz. Maximum switching contrast of 0.6 was achieved at ~ 0.6 THz for all three metadvice as shown in figure 3(c). Hence, a simple cantilever array fabricated on lightly doped Si substrate acted as an efficient THz switch. The geometrical parameters of the cantilevers and the thickness of constituent materials could be engineered to achieve desired tunable THz response. Electrostatic actuated cantilever array was also reported for continuous spectral tunability of resonance frequency, by gradually varying the gap between the substrate and the released cantilevers [119]. In another report, simultaneous tuning of multiband resonance was demonstrated using triple cantilever resonator as a unit cell of the THz MEMS metadvice [120].

The simplicity of cantilever design and integration allows for selectively releasing a part of any resonator design and then by electrically connecting them will enable active structural reconfiguration using electrostatic actuation. Hence, the cantilever approach was reported for a wide range of reconfigurable THz functionalities. In an initial work, the side arms along with the tip arms of dual SRR unit cell were released to form 'L'-shaped cantilevers as shown in figure 3(d), to enable electrostatically tunable magnetic response at THz frequencies [121]. Alternatively, active control of resonant electrical response was reported by releasing the 'T'-shaped cantilever formed from the centre arms along with the capacitive tip arm of the ESRR unit cell as shown in figure 3(e) [122, 123]. Furthermore, polarization independent response was also reported for all reconfiguration states using a unique metamaterial unit cell design that consisted of eight cantilevers placed at each corner of electrically connected octagon ring, as shown in figure 3(f). The metadvice response for both E_x and E_y polarized THz incidence were identical at all reconfiguration states [124]. This was achieved due to the high symmetry of octagon-shaped unit cell design as well as the out-of-plane reconfiguration of cantilevers, which preserves the symmetry of unit cell in all states. Electrostatic cantilever integrated metadvice was also reported for dynamic polarization control of THz waves [125]. The unit cell design consisted of cantilever array that can be reconfigured to come in contact with an orthogonally oriented metal line as shown in figure 3(g). The metadvice response for THz incidence polarized along the cantilever length was varied strongly, while the metadvice response for orthogonal polarization remained relatively unchanged. This anisotropic response was then utilized to dynamically alter the polarization of THz waves between circular and linear states.

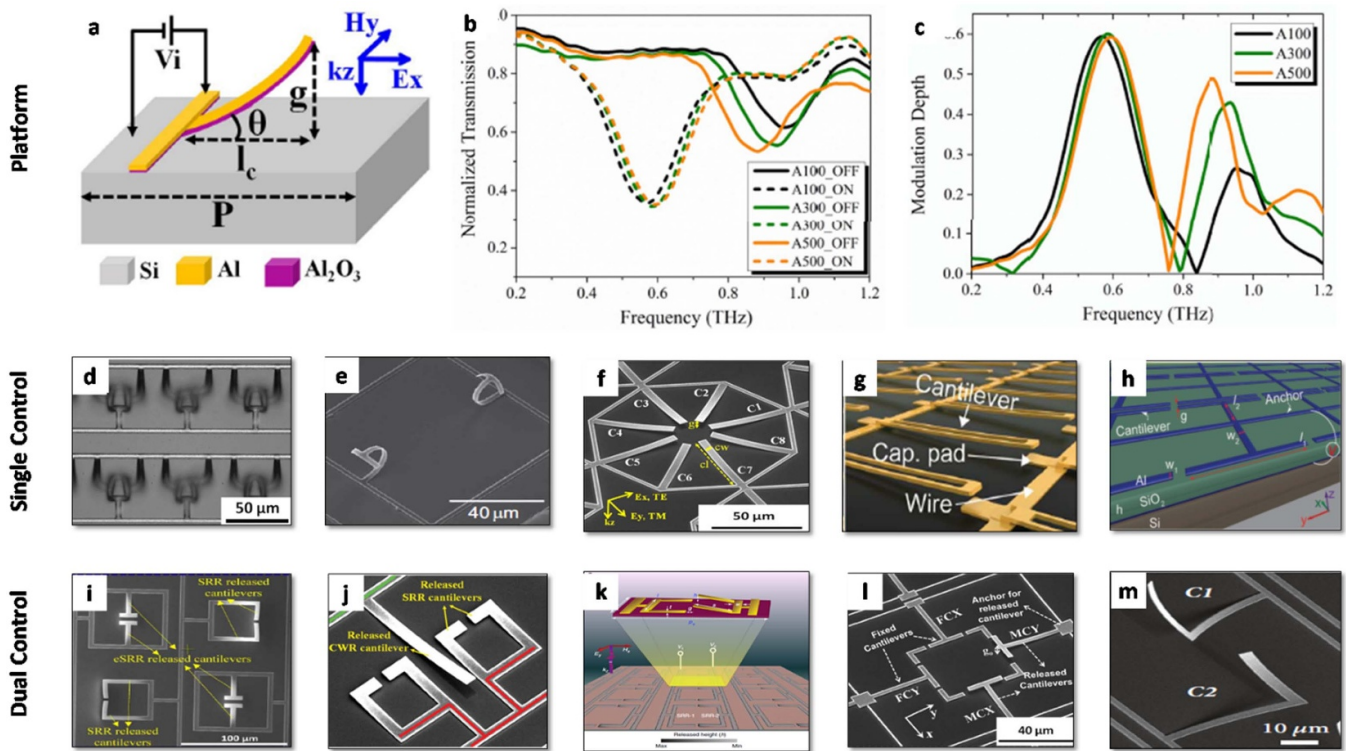


Figure 3. Electrostatically reconfigurable cantilever-based THz MEMS metadevices. (a) Schematic of prestressed bimaterial cantilever fabricated on lightly doped Si substrate, (b) THz transmission spectra of the cantilever metadvice with varying thickness of Al layer—100 nm, 300 nm and 500 nm in ON and OFF state, respectively and (c) corresponding modulation depth of the cantilever metadvice. © [2015] IEEE. Reprinted, with permission, from [118]. The bimaterial cantilever platform with global control was adopted for active control of various THz response—(d) magnetic response, reprinted from [121], with the permission of AIP Publishing, (e) electrical response reproduced from [123]. CC BY-NC-SA, (f) polarization-insensitive resonance switching reproduced from [124]. CC BY 4.0., (g) polarization control reproduced with permission from [125] and (h) phase control [126] John Wiley & Sons. © 2017 WILEY-VCH Verlag GmbH & Co. KGaA, Weinheim. The electrostatic cantilever platform also allowed for dual independent control and this allowed for advanced manipulation of terahertz response—(i) independent switching of magnetic and electric response reprinted with permission from [130] © The Optical Society, (j) modulation and tuning of electromagnetically induced transparency analogue [131] John Wiley & Sons. © 2016 WILEY-VCH Verlag GmbH & Co. KGaA, Weinheim., (k) out-of-plane symmetry broken Fano resonances reproduced from [132]. CC BY 4.0, (l) complete control of linear anisotropy [134] John Wiley & Sons. © 2015 WILEY-VCH Verlag GmbH & Co. KGaA, Weinheim and (m) chirality switching reproduced from [135]. CC BY 4.0.

Furthermore, electrostatic cantilever was also integrated in a metal–insulator–metal (MIM) cavity configuration as shown in figure 3(h) for dynamic phase control [126]. The array of cantilevers formed the top metamaterial layer, while the bottom reflector was formed by a continuous Al film on Si substrate. The spacer layer was a stack of thick SiO₂ layer, 50 nm thin Al₂O₃ layer and a tunable air gap. Hence, by applying the voltage between the bottom Al and top cantilever, the air gap and consequently the effective spacer thickness was dynamically varied. This allowed for the switching of metadvice between over-damped and under-damped regions with corresponding phase span of full 360° and less than 180°, respectively. Such level of dynamic phase control was reported to enable THz polarization control, beam steering and holographic beam forming applications through simulation studies [127]. The MIM architecture with metamaterial as top layer was also reported for tunable THz absorption [128]. The metadvice unit cell consisted of ‘I’-shaped resonator fabricated on SiN membrane that was suspended with two cantilevers that were anchored to a fixed rectangular ring. The air gap between

the top metamaterial layer and bottom reflector was reduced by applying voltage between them and this led to the gradual red-shifting of peak absorption frequency of the THz MEMS metadvice.

The fabrication process used to realize electrostatic cantilever readily allows for two isolated electrical control of the metadvice [129]. This opened a new avenue for advanced manipulation of THz waves as shown in figures 3(i)–(m). In the initial report, electrically isolated SRR and ESRR unit cells placed in an interpixelated fashion as shown in figure 3(i), was reported for independent control of magnetic and electrical resonances [130]. Then, independent reconfiguration of bright and dark mode resonators in near-field coupled metadvice was reported for amplitude modulation and spectral tuning of electromagnetically induced transparency (EIT) analogue as shown in figure 3(j) [131]. Similar approach was also employed for the realization of Fano resonance through symmetry breaking in the wave propagation direction [132]. Two SRRs with independent control formed the Fano resonator unit cell as shown in figure 3(k). By changing the height of

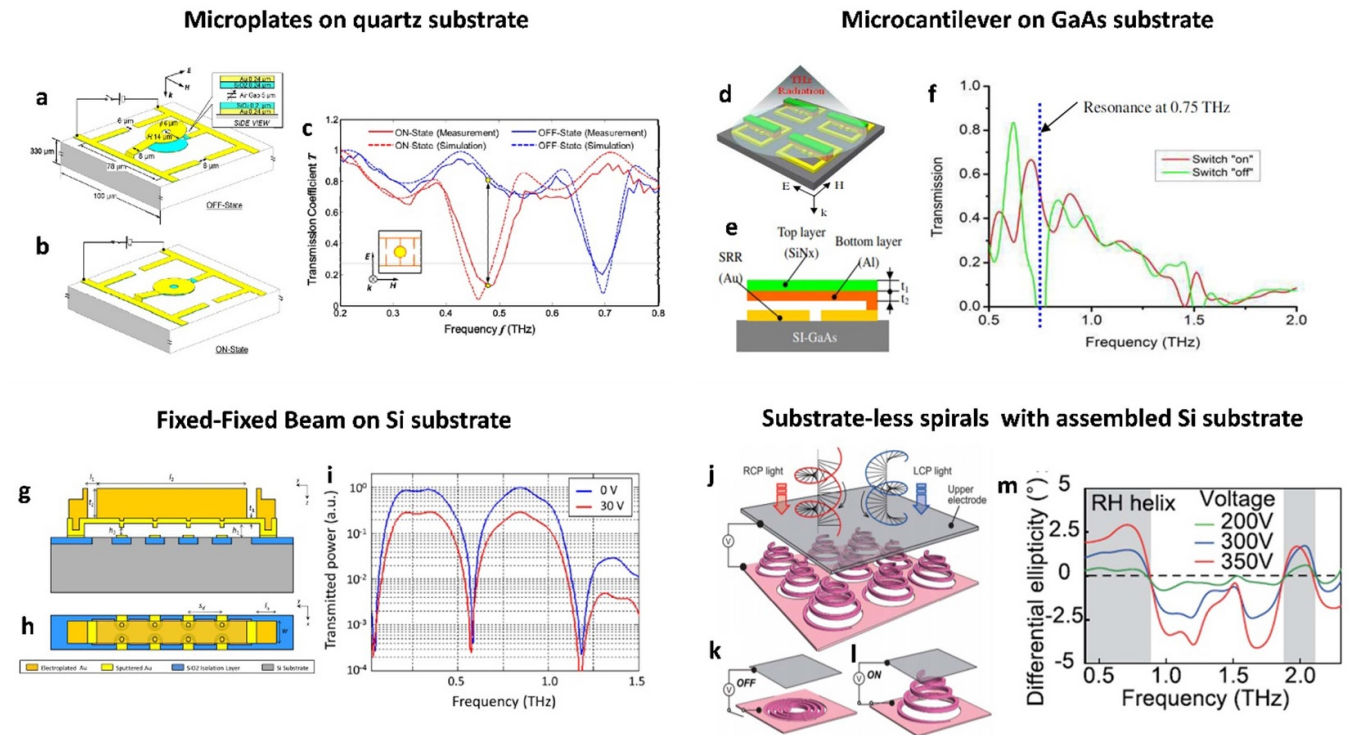


Figure 4. Alternate electrostatic actuator designs for out-of-plane reconfigurable THz MEMS metadevices. (a), (b) Metallic microplate cantilever fabricated on quartz substrate with bottom metal fixed on the substrate in OFF and ON states, respectively and (c) corresponding measured and simulated THz transmission spectra of the microplate metadvice in ON and OFF states. Reprinted with permission from [140] © The Optical Society. (d) Schematic of Al/SiNx cantilevers fabricated over ESRR metamaterial on GaAs substrate, (e) cross-sectional view of the metadvice schematic and (f) measured THz transmission spectra of the metadvice in ON and OFF states [142] reproduced courtesy of The Electromagnetics Academy. (g) Cross sectional view and (h) top view of the electrostatically driven fixed-fixed beam on orthogonally placed metallic strips and (i) corresponding THz transmission spectra of the metadvice in ON and OFF states reprinted with permission from [144] © The Optical Society. (j) Schematic of out-of-plane reconfigurable substrate-less spirals by assembling another Si substrate on top as actuation electrode, (k), (l) shows the schematic of unit cell in OFF and ON states, respectively and (m) corresponding differential ellipticity measured for various voltages between the released metallic spirals and assembled Si substrate. Reprinted from [146], with the permission of AIP Publishing.

the cantilevers in each SRR independently, the strength of the Fano resonance was modulated. Interestingly, the presence of Si substrate broke the mirror symmetry of the metadvice in the vertical direction and enabled metahysteresis behaviour. This unique feature was used for demonstrating various logic gate operations at THz frequencies [132, 133]. In another work, complete control of anisotropic response was reported by isolating the control to orthogonally twisted cantilevers placed in a ring resonator configuration as shown in figure 3(l) [134]. Based on the combination of cantilever switched and polarization of incident THz waves, varied linear polarization response was achieved at specific THz frequency. Active switching of chirality between achiral, levorotatory, dextrorotatory and racemic states was also reported by using isolated control of orthogonally twisted 'L'-shaped cantilevers as metadvice super cell as shown in figure 3(m) [135]. Various other functionalities were also reported using the electrically isolated electrostatic cantilever platform including switching of EIT analogue in tri-atomic metadvice [136], THz bandwidth control [137], tunable filter [138], and tunable dual band absorption [139]. The two lithography step fabrication process limits the control to only two isolated electrodes for a metadvice. However, the number of metallic layers can be

scaled up and this will enable even higher level of isolation for extreme THz wave manipulation.

Even though the microcantilever on doped Si substrate enables simpler implementation of electrostatically driven THz metadvice, it suffers from additional loss due to substrate doping, limited reconfiguration range, and reduced reliability. Alternative electrostatic schemes for out-of-plane reconfiguration are also explored to address the aforementioned challenges. Electrostatically actuated microplate array, fabricated on quartz substrate was reported to perform as an efficient THz filter and modulator [140, 141]. The metadvice unit cell consisted of two SiN coated Au plates—one fixed on the quartz substrate, while the other was suspended above the fixed plate with an air gap between them (OFF-state), as shown in figure 4(a). When voltage was applied between the two Au plates, the electrostatic force pulls the suspended plate towards the fixed plate. Beyond the critical pull-in voltage, the gap between the two plates was completely closed (ON-state), as shown in figure 4(b). Thin coating of SiN dielectric on both Au plates prevents the electrical short between the two Au plates upon physical contact. The metadvice showed a large switching contrast of over 70% at 0.48 THz for an applied voltage of ~ 33 V, as shown in figure 4(c). The large surface area of

the plates enabled lower actuation voltage, even with a large air gap between the two plates of $\sim 5.8 \mu\text{m}$. Such large gaps are required to achieve high enough restoring force that would overcome the adhesion forces of the SiN coated Au plates, and bring the cantilevers back to their initial OFF state. This is important for ensuring repeatable operation of the electrostatically driven THz MEMS metadevices. Also, the use of quartz substrate alleviated the substrate related loss incurred in doped Si substrate based metadevices. In another report, Al/SiN bimaterial cantilevers were fabricated on top of the Au ESRR on semi insulating gallium arsenide (GaAs) substrate as shown in figures 4(d) and (e). Electrostatic actuation was used to electrically short the ESRR gap by pulling down the cantilever [93, 142]. This allowed for the dynamic switching of LC resonance at 0.75 THz with a contrast of over 50% as shown in figure 4(f). Integration of THz MEMS on GaAs substrate could also be used for reconfigurable THz sources and detectors. Complementary to fixed-free cantilevers, electrostatically driven fixed-fixed beams were also reported for the realization of THz MEMS metadevices [143, 144]. In this report, vertically aligned Au beam was suspended over horizontally aligned Au lines that were fabricated on SiO₂ coated Si substrate as shown in figures 4(g) and (h). When voltage was applied between the suspended Au beam and Si substrate, the vertically and horizontally aligned Au lines came in contact and were electrically shorted, thereby forming a 2D mesh pattern. This allowed for the broadband THz modulation of 70% at 30 V for a bandwidth of over 1.5 THz, as shown in figure 4(i). A variant of fixed-fixed beam, which is a membrane suspended by anchors was reported for spectrally tunable THz absorbers [145]. In all of the aforementioned approaches, the deformation range is quite limited due to the achievable thickness of sacrificial layers and the direction of actuation is always towards the substrate due to the attractive nature of electrostatic actuation. For certain applications, such as chirality switching, spiral microstructures need to be reconfigured between planar 2D spirals to 3D helices. To realize such large deformation, a novel scheme was reported by assembling a Si substrate in front of released spiral cantilevers with desired gap between them [146]. Upon applying voltage between the assembled Si substrate and suspended spiral cantilevers, the as-fabricated planar spirals were reconfigured into a 3D helices with a strong switching of chiral response, as shown in figures 4(k)–(m) respectively. All of the aforementioned works clearly highlight the key advantages of electrostatic actuation, including simpler integration, versatile design, low power operation and multichannel control to enable wide range of high-performance THz MEMS metadevices.

2.2.2. In-plane electrostatic reconfiguration. Comb drive actuator is the most popular choice of electrostatic actuators that enable large in-plane deformation [147]. Comb drive actuator consists of a pair of interdigitated overlapping fingers, in which one set of fingers is free to move, while the other set remains fixed. When voltage is applied between the two sets of fingers, the electrostatic field between the fingers drives the

movable set along the in-plane direction. Electrostatic comb drive actuators can provide continuous and large displacement and hence have been extensively used for in-plane reconfigurable THz MEMS metadevices [148]. In an initial report, a pair of SRRs formed a unit cell of which one SRR was fabricated on a movable Si frame driven by electrostatic comb drive actuators, while the other SRR was fabricated on the fixed Si island, as shown in figures 5(a) and (b) [149]. The SRR housed on the frame could then be moved either towards or away from the fixed SRR, thereby forming either an opening state, closed-ring state or back-touch state configuration of the unit cell, as shown in figures 5(c)–(e), respectively. The bidirectional reconfiguration was achieved by using two comb drive actuators fixed on either sides of the movable Si frame, as shown in figure 5(a). The as-fabricated metadvice unit cell consists of two SRRs with two capacitive gaps on either sides, as shown in figure 5(b). When THz wave with TE polarization was incident at 45°, Fano-type magnetic resonance was observed at ~ 2.12 THz, as shown in figure 5(f). By increasing the capacitive gap from 2 μm to 6 μm between the SRRs, the resonance frequency was blue-shifted from 2.12 to 2.28 THz, respectively, as shown in figure 5(f). When the in-plane gap between the SRRs was completely closed i.e. close-ring state, no resonance was observed as shown in figure 5(g). Similarly, when back-touch configuration was formed by actuating the SRR in opposite direction, no resonance was observed as well, as shown in figure 5(h). Hence, the in-plane reconfiguration allowed for switching of magnetic resonance as well as spectral tuning of magnetic resonance frequency of the THz MEMS metadvice. The versatility of this platform allowed for the active control of various THz functionalities. Anisotropy switching was reported in a maltase cross metamaterial driven by comb-drive actuator [150]. This was realized by selectively breaking the symmetry of the cross structure along one-direction, while preserving it along the orthogonal direction in all reconfiguration states as shown in figure 5(i). In another work, the THz response of the metadvice was actively switched between polarization-dependent state and polarization-independent state by altering the lattice constant of the unit cells through in-plane reconfiguration as shown in figure 5(j) [151]. The as-fabricated metadvice had varying pitch along x -direction and y -direction and showed polarization-dependent THz response. Alternate lines of the metamaterial were fabricated on a movable frame connected to a set of comb drive actuators. By changing the relative position of the unit cells in the neighbouring lines, the lattice period was shifted to form interpixelated supercell with four fold-rotational symmetry and hence led to polarization-independent THz response. The comb drive integrated THz MEMS metadvice was also reported for polarization conversion and rotation by forming staircase structures with UP, 'T' and DOWN states [152]. The metamaterial consists of horizontal metallic slabs on fixed Si islands and the vertical metallic slabs were fabricated on the movable Si frame. By selectively displacing the vertical slabs, the staircase structure could be reconfigured between the UP, 'T' and DOWN states as shown in figure 5(k). The polarization rotation angle was reconfigured between -12.8° , 0° and $+13.1^\circ$ at 1.78 THz

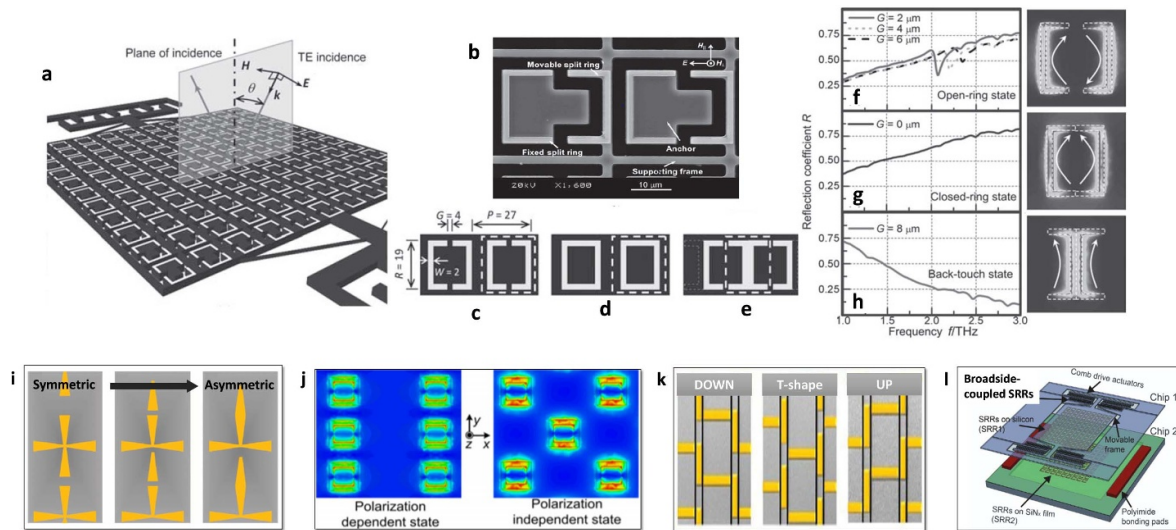


Figure 5. Electrostatic in-plane reconfigurable THz MEMS metadevices. (a) Schematics of dual SRR metadvice, where one SRR is fabricated on the fixed Si island, while the other on a movable Si frame driven by comb drive actuators, (b) SEM image of the fabricated unit cells, the schematic representation of various reconfiguration states of the dual SRR realized using comb drive actuators—(c) as-fabricated open-ring state, (d) closed-ring state and (e) back-touch state and the measured reflection spectra of the dual SRR—(f) in open-ring state with varying in-plane capacitive gap between the SRRs, (g) closed-ring state and (h) back-touch state, respectively. [149] John Wiley & Sons. Copyright © 2011 WILEY-VCH Verlag GmbH & Co. KGaA, Weinheim. Electrostatic comb drive actuation has been used for active control of various THz functionalities—(i) tunable anisotropy reproduced from [150]. CC BY 4.0., (j) switching between polarization-dependent and polarization-independent states. Reprinted from [151], with the permission of AIP Publishing, (k) polarization rotation. Reproduced from [152]. CC BY 4.0 and (l) broadside coupling between SRRs. Reproduced from [153]. CC BY 4.0

corresponding to UP, 'T' and DOWN states of the staircase unit cell. Comb drive actuators were also reported for dynamic control of broadside coupling in dual layer SRRs [153]. The metadvice consists of two arrays of SRRs stacked in a broadside-coupled manner [154]. The unit cell consists of a pair of 180° rotated SRRs separated by an out-of-plane gap as shown in figure 5(l). Due to broadside coupling, mode splitting was observed. When the relative overlap between the two SRRs was varied, a large blue-shift in symmetric mode and large red-shift in anti-symmetric mode was observed. Furthermore, strong amplitude modulation and phase shift were also achieved at specific THz frequency. Comb drive based THz MEMS metadevices have also been reported for reconfiguration of in-plane coupling in asymmetry SRRs [148]. In a more recent work, comb drive integrated substrateless metadvice was also reported for active tuning of EIT analogue [155]. Hence, comb drive actuators provide a powerful platform for in-plane reshaping of metamaterial unit cell geometry as well as lattice reconfiguration to achieve versatile THz functionalities.

2.3. Piezoelectric reconfiguration

Piezoelectric materials possess non-centrosymmetric crystal-line structure that enables mechanical expansion or contraction, depending on the polarity of applied voltage. Some of the popular piezoelectric materials used for MEMS actuators include PZT, AlN, ZnO and PVDF. Piezoelectric actuators can provide continuous as well as bidirectional reconfiguration. Piezoelectric actuator housing released SRRs or in microgripper configuration for in-plane reconfigurable THz metadevices

have been theoretically proposed [156, 157]. However, experimental demonstration has not yet been reported, owing to the complexity in piezoelectric MEMS device fabrication. Also the in-plane displacement enabled by piezoelectric actuation could be very minimal and might be a challenge in realizing high performance THz MEMS metadevices [156]. A more practical approach will be to use piezoelectric actuation for out-of-plane reconfiguration by adopting bimaterial cantilever configuration. The bimaterial cantilever can be made of a stack of piezoelectric and elastic layers. When voltage is applied across the piezoelectric layer, it will either expand or contract based on the polarity of the applied electric field, while the elastic layer will remain unchanged. This will lead to an overall out-of-plane deformation of the bimaterial cantilever. Such bimaterial cantilevers can be incorporated into metamaterial unit cell geometry for active control of THz response. Also, bimaterial cantilevers can also be made with oppositely polled piezoelectric layers to enable larger out-of-plane displacement for a given voltage. Piezoelectric actuation provides electrically controlled bidirectional and continuous reconfiguration, lower operational power, higher speed and can be realized using CMOS compatible processes. Currently, the exploration of piezoelectric actuation for THz metadvice is largely limited by the complexity in fabrication process, but has the potential of becoming a competitive approach for realizing efficient THz MEMS metadevices.

2.4. Electroactive polymer-based reconfiguration

Electroactive polymer based actuators have been widely used for soft robotics. π -conjugated polymer based actuator

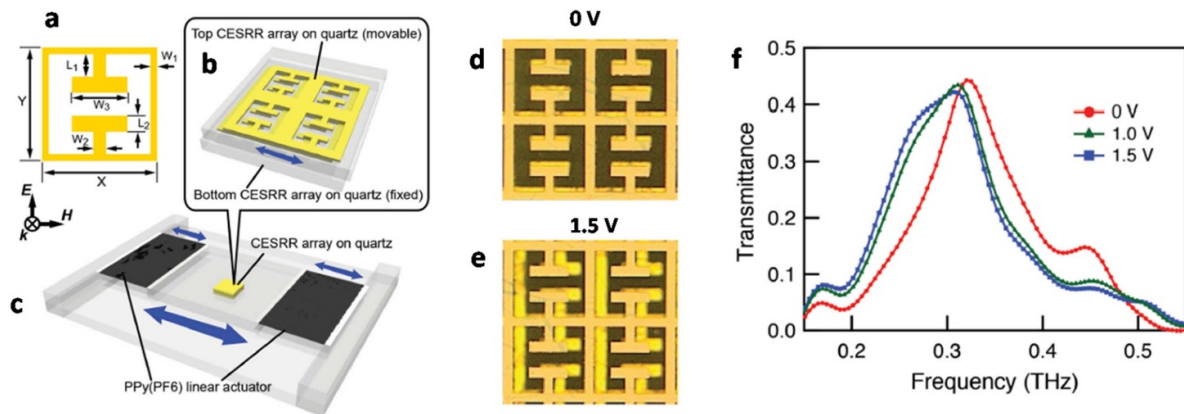


Figure 6. Electroactive polymer based THz MEMS metadvice. (a) Schematic of complementary ESRR (CESRR) unit cell with geometrical parameter definitions. (b) Schematic of assembled dual CESRR with top CESRR array on quartz suspended over the fixed bottom CESRR array on quartz substrate. (c) Schematic of entire THz MEMS metadvice with top CESRR array on quartz attached to ppy(PF6) linear actuator on either sides to provide in-plane reconfiguration upon applying voltage. OM images of the fabricated out-of-plane coupled CESRR metadvice at (d) 0 V and (e) 1.5 V, respectively. (f) Measured THz transmission spectra of the in-plane reconfigurable dual CESRR metadvice at varying voltages. [158] John Wiley & Sons. © 2015 WILEY-VCH Verlag GmbH & Co. KGaA, Weinheim.

works on the principle of electrochemical reduction-oxidation (redox) reaction. By applying voltage, doped ions can be moved into and out of the π -conjugated polymer based on the polarity of the applied voltage. This movement of ions makes the polymer to either expand or contract in a reversible manner. Heavily doped polypyrrole (PPy) film based linear actuator was adopted for in-plane reconfigurable THz MEMS metadvice [158]. The metadvice consists of two complementary ESRR (CESRR) metamaterials fabricated on quartz substrates and were assembled on top of each other with a small gap between them, as shown in figures 6(a) and (b). The suspended CESRR metamaterial was attached to the PPy linear actuators on either sides, which provided bidirectional in-plane reconfiguration in response to the applied voltage, as shown in figure 6(c). When no voltage was applied (0 V), the two CESRRs were perfectly aligned, as shown in figure 6(d). The symmetric mode of the metadvice was observed at 0.32 THz, as shown in figure 6(f). Upon applying an input voltage of 1.5 V, the top CESRR metamaterial was laterally shifted, resulting in misalignment between the two CESRR metamaterials, as shown in figure 6(e). The symmetric mode of the metadvice at 1.5 V was red shifted to 0.3 THz, as shown in figure 6(f). Electroactive polymer based origami actuator was also shown to tune the out-of-plane coupling gap between the metamaterials. Hence, electroactive polymers have the potential to enable large in-plane as well as out-of-plane reconfiguration at relatively small voltages and is attractive for a wide range of THz MEMS metadices.

2.5. Pneumatic reconfiguration

Pneumatic actuation is realized by creating a pressure difference across substrate-free microstructures. Large, continuous and bi-directional deformation of microstructures have been shown using pneumatic actuation. Pneumatics driven THz MEMS metadvice has been reported for chirality

switching [159]. The metamaterial consists of an 2D array of released planar Archimedean spiral, as shown in figure 7(b). The fabricated spiral metadvice was housed in a pressure chamber that could provide reversible pressure difference in the out-of-plane direction. When the pressure below the metadvice was increased, the 2D spirals moved upward and transformed into right-handed (RH) 3D helices, as shown in figure 7(a). For the pressure difference of 10 Pa, maximum deformation at the tip was measured to be as high as 60 μm , as shown in figure 7(c). When the pressure gradient was reversed, the planar spirals deformed downward by $\sim 60 \mu\text{m}$ to form left-handed (LH) 3D helices, as shown in figure 7(c). Total deformation range of 120 μm was achieved using the pneumatic actuation. Such large deformation is important for strong chirality switching, as the range of spiral deformation determines the modulation of polarization state of THz wave passing through the metadvice as schematically shown in figure 7(b). A large tunable ellipticity between $+28^\circ$, 0° to -20° was achieved at 1.1 THz, corresponding to the reconfiguration states of RH, planar and LH helices, as shown in figure 7(d). In another work, pneumatic actuation was reported for active tuning of resonance frequency for orthogonal linear polarizations of incident THz waves [160]. The metamaterial unit cell consisted of electrically coupled asymmetric SRRs that were placed with a sub-micron gap between them. One of the SRRs was fabricated on the fixed membrane, while the other SRR was fabricated on a microcantilever that is connected with a zigzag anchor. Upon applying air pressure across the metamaterial, the movable SRR was deformed in the out-of-plane direction by over 5 μm for 1 kPa of pressure. The corresponding spectral shift of 0.1 THz was achieved for both polarizations of incident THz. Hence, pneumatic actuation has shown to provide significantly large, bidirectional and continuous deformation, as well as eliminates the need of metallic interconnects. This will be valuable for niche THz applications, such as chirality-based chemical sensors, THz polarizers and table-top spectrometers.

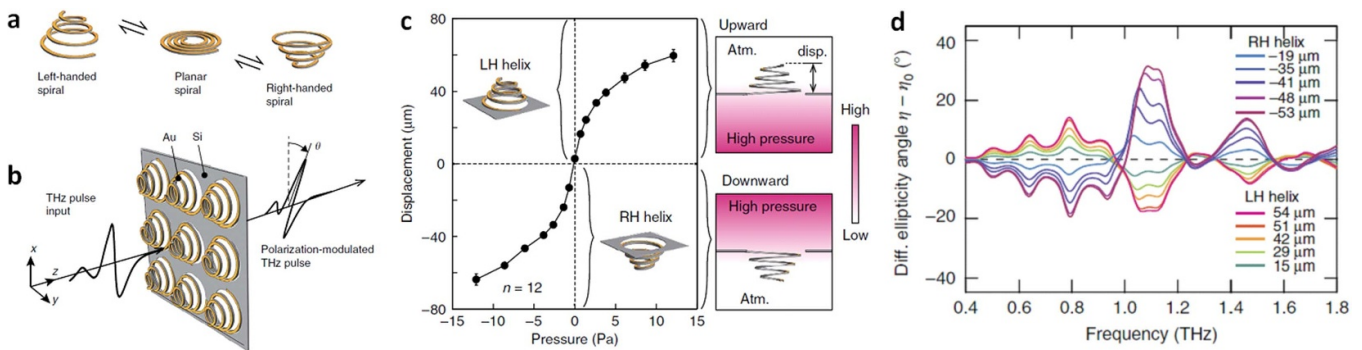


Figure 7. Pneumatics driven THz MEMS metadvice. (a) Schematics of different reconfiguration states of spiral metamaterial unit cell—left-handed spiral, planar spiral and right-handed spiral. (b) Schematic representation of polarization-modulation of incident terahertz wave by controlling the handedness of spiral array. (c) Measured upward and downward displacement of spiral with increasing pressure difference on either direction. (d) Measured differential ellipticity angle of chirality switching metadvice with varying deformation of right-handed helix and left-handed helix using pneumatic actuation. Reproduced from [159]. CC BY 4.0.

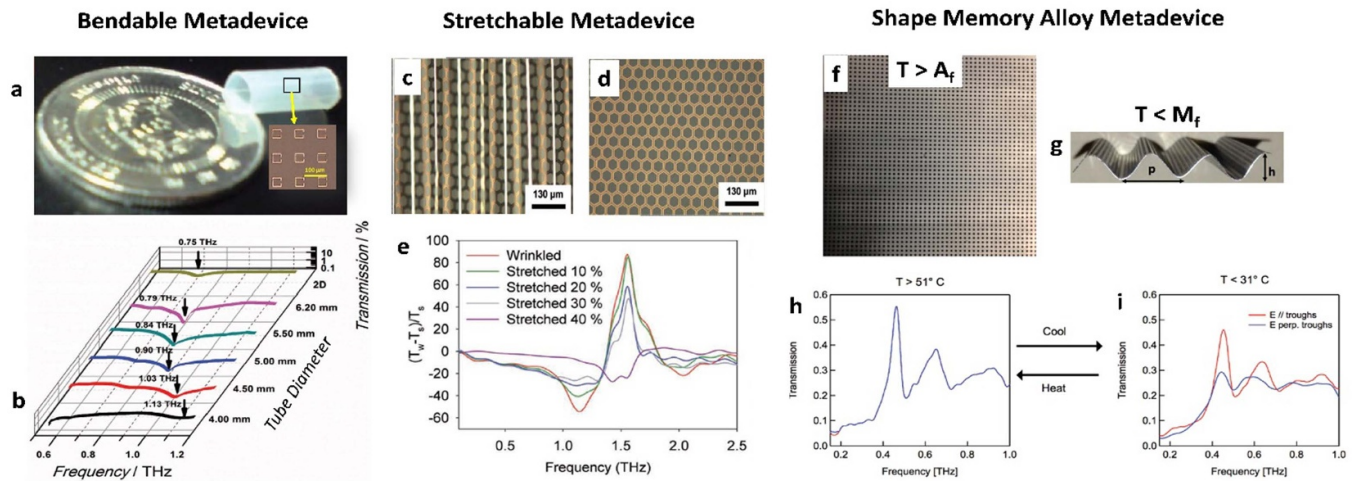


Figure 8. Mechanically reconfigurable THz MEMS metadvice. (a) Fabricated THz SRR metadvice on flexible substrate and rolled into a tube form. (b) Measured THz response of the rolled-up metadvice with varying tube diameter. [173] John Wiley & Sons. Copyright © 2012 WILEY-VCH Verlag GmbH & Co. KGaA, Weinheim. (c) Stretchable honeycomb metamaterial fabricated on pre-strained PDMS substrate that wrinkles upon releasing and (d) completely stretched-out metamaterial after applying 52.5% strain and (e) differential THz transmission of wrinkled and variably stretched metadvice relative to fully stretched (flat) metadvice. [182] John Wiley & Sons. Copyright © 2012 WILEY-VCH Verlag GmbH & Co. KGaA, Weinheim. (f) Plasmonic THz hole array formed on shape memory alloy film at temperature higher than A_f and (g) sinusoidal curved metadvice by cooling the metadvice below M_f , (h), (i) measured THz transmission response of flat metadvice and 1D sinusoidally curved metadvice for orthogonal polarization of THz incidences, respectively. [185] John Wiley & Sons. © 2017 WILEY-VCH Verlag GmbH & Co. KGaA, Weinheim.

2.6. Mechanical reconfiguration

Flexible substrates provide a direct means of achieving mechanical reconfigurability either by bending or stretching the substrate housing the metamaterial. Wide range of metamaterials fabricated on mechanically deformable flexible substrates were reported for active THz control [161]. Different flexible substrates, THz resonator designs and reconfiguration schemes have been reported for various functional metadvice and are discussed in this section.

2.6.1. Curvature-based reconfiguration. The primary property of any flexible substrate is the ability to bend upon applying mechanical force. Some of the popular flexible substrates used for THz metamaterials include polyimide [17,

31, 69, 73, 162–166], polydimethylsiloxane (PDMS) [167–170], polyethylene terephthalate (PET) [50, 171], parylene [172], polyethylene naphthalate (PEN) [173, 174], polypropylene [175], silicone [176] and silk [177–180]. In an initial work, metallic SRRs fabricated on PEN substrates were rolled into 3D tubes with varying diameter, as shown in figure 8(a) [173]. The resonance frequency of the planar SRR was measured at 0.75 THz, as shown in figure 8(b). When the metadvice was rolled into 3D tubes with decreasing diameter, the resonance frequency gradually blue shifted to 1.13 THz for the diameter of 4 mm, as shown in figure 8(b). In addition, the hollow core of the metamaterial was replaced with dielectric materials and the change in THz resonance frequency was used to estimate the refractive index of the core material. The high sensitivity of the metamaterial allowed

for the detection of minuscule refractive index change of ~ 0.0075 . In another work, symmetric Au ESRR metamaterial was sandwiched between two PDMS layers and upon bending, the resonance frequency of the metadvice gradually blue shifted with increasing curvature [181]. Hence, bending of flexible substrates provides an straightforward means of achieving reconfigurability without the need for active materials, complex processing or electrical interconnections. They also enable extremely low-loss and low-cost metadvice.

2.6.2. Strain-based reconfiguration. A subset of flexible substrates such as PDMS are elastic in nature and hence expand upon applying in-plane strain. This property of elastic substrates has also been used for realizing in-plane reconfigurable THz metadvice [168, 169, 182, 183]. Hexagon-shaped metallic resonators in honeycomb lattice were fabricated on a thin polyimide substrate and were then transferred to a pretrained PDMS substrate. Upon releasing the strain, the PDMS layer with metallic resonators wrinkled up, as shown in figure 8(c) [182]. Mechanical strain of 52.5% was applied to flatten the wrinkled layout as shown in figure 8(d). The relative change in THz transmission at 1.5 THz was changed continuously and a maximum change of 80% was observed between the as-fabricated wrinkled and strain-applied flat layout of the metadvice, as shown in figure 8(e). Similarly, closely spaced 'I'-shaped resonators, fabricated on PDMS substrate was also reported for mechanically reconfigurable THz response [168]. Upon applying mechanical strain, the intercell capacitance along the length of 'I' direction decreased, thereby causing the resonance frequency of the metadvice to red shift. The spectral tunability of the metadvice was improved by adopting a corrugated 'I'-shaped resonator, which provided larger intercell capacitance compared to the plain 'I'-shaped resonators. The 'I'-shaped metadvice were polarization sensitive. To enable polarization insensitive response, a cross resonator with corrugated capacitive gaps was reported [169, 184]. Hence, mechanically stretchable substrates provide a simpler route to achieve in-plane reconfigurable metadvice, that are essential for applications demanding non-conformal coatings, such as wearable devices and stealth technologies.

2.6.3. Shape memory alloy (SMA) for reconfiguration. SMAs are phase transition materials that can be switched between two stable phases in response to applied temperature. One such SMA is nitinol (NiTi), a metal alloy composed of approximately equal atomic percentages of nickel (Ni) and titanium (Ti). NiTi shows phase transition between the martensite phase below the transition temperature and the austenite phase above the transition temperature, respectively. The phase transition temperature of NiTi is close to room temperature. NiTi also has very high DC conductivity of $\sim 1.2 \times 10^6 \text{ S m}^{-1}$ in both the states. Hence, subwavelength-sized holes perforated in NiTi was reported as a phase transition powered THz metadvice [185]. The SMA was trained to achieve both 1D and 2D sinusoidal corrugation upon phase transition. When the applied temperature was lower than the martensite phase transition temperature, the NiTi hole array

formed a 1D sinusoidal pattern as shown in figure 8(g). This resulted in polarization-dependent THz transmission response for $E||$ and E_{perp} incidence of THz waves with transmission amplitude of ~ 0.45 and 0.25 , respectively, as shown in figure 8(i). When the temperature was raised above the austenite phase transition, the NiTi metadvice became flat as shown in figure 8(f). The corresponding THz response was polarization-independent for both $E||$ and E_{perp} THz incidence with maximum transmission of ~ 0.55 at 0.45 THz as shown in figure 8(h). Similarly, an aperture was formed in the NiTi film and was trained to have 2D sinusoidal corrugation around the aperture in the martensite phase. The THz transmission was increased to almost unity at 0.1 THz , while for the bare aperture on a flat NiTi film, the transmission was only 0.45 THz . Hence, phase transition in SMA was shown to be an efficient platform to achieve THz MEMS metadvice with memory effects and trainable properties.

2.7. Microfluidic reconfiguration

Microfluidics integrated with THz metamaterials have been widely reported for sensing applications [186–190]. Interestingly, microfluidic metamaterials are also reported for THz metadvice by injecting controlled proportion of liquid metal into the microchannels [191, 192]. In an initial work, two layers of 'S'-shaped microfluidic channels were orthogonally twisted with respect to each other and separated by $100 \mu\text{m}$ thick PDMS layer formed a microfluidic THz metadvice, as shown in figures 9(a) and (b) [193]. By filling the two channels with different refractive index materials such as mercury and air, strong optical activity was achieved at 2.56 THz . Alternatively, the polarization rotation of the metamaterial was also tuned, by injecting the top 'S' layer of the metamaterial with varying concentration of sodium chloride (NaCl) solution, while the bottom layer was filled with mercury. Maximum rotation angle of 16.9° was achieved for 0% NaCl. With increasing NaCl concentration, the polarization rotation angle gradually reduced and reached 0° at 16% NaCl concentration as shown in figure 9(c). In another work, eutectic gallium indium (EGaIn) was used as the liquid metal to realize THz metadvice [194]. The shape of the injected EGaIn was mechanically stabilized by the formation of a thin oxide surface layer that allowed the fluid to maintain its configuration within the microchannel despite its high intrinsic surface energy. The EGaIn could be flowed again by increasing the intrinsic pressure to go beyond the critical value. This allowed for the reshaping of THz resonator between SRR, closed ring resonator and irregular closed ring resonator geometries as shown in figures 9(d)–(f), respectively. Each of these configurations, provided starkly different THz response. Alternatively, array of liquid metal pillars of varying heights was formed using microfluidic approach and was demonstrated to achieve polarization independent, frequency agile and wide angle THz absorption as shown in figures 9(g) and (h) [195, 196]. By increasing the liquid metal height from 30 to $90 \mu\text{m}$, the peak absorption frequency was tuned from 0.246 to 0.415 THz , which provided a large tuning range of 51.1% as shown in figure 9(i). For a wide angle of incidence from 0° to 60° ,

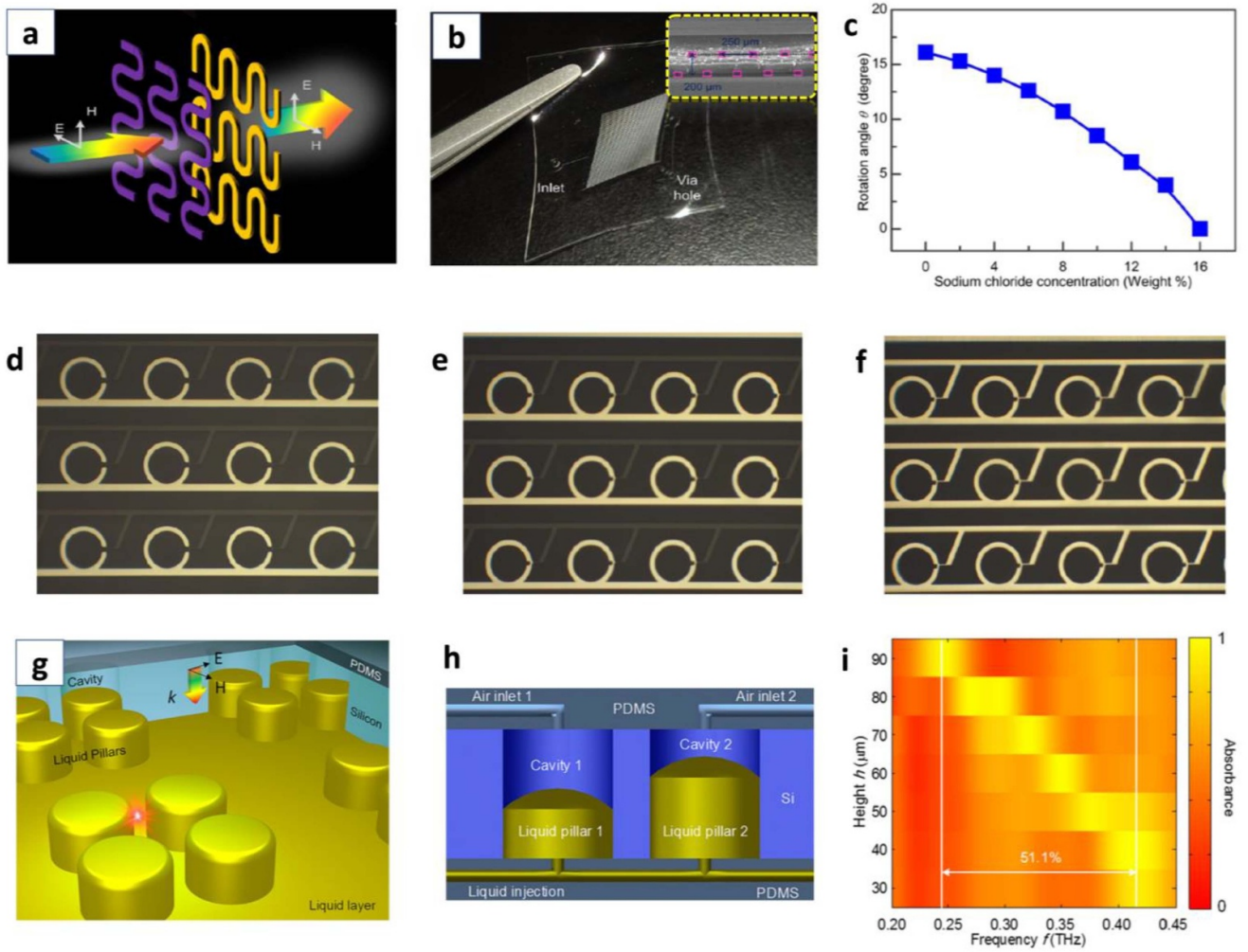


Figure 9. Microfluidics integrated THz MEMS metadevices. (a) Schematic representation of polarization rotation in a two-layered ‘S’-shaped microfluidic metadvice separated by thin PDMS layer, (b) optical image of the fabricated metadvice and the inset showing two microfluidic channels, highlighted in pink colour and (c) change in polarization rotation angle when filled with mercury on bottom metamaterial, while the top metamaterial was filled with varying concentration of sodium chloride solution. © [2014] IEEE. Reprinted, with permission, from [193]. (d)–(f) Eutectic Gallium Indium liquid metal filled in microfluidic channel with retention of shape, leading to the formation of open SRR, closed ring resonator and irregular closed ring resonator, respectively. Reprinted with permission from [194] © The Optical Society. (g) Schematic of liquid metal filled pillar metamaterial for terahertz absorption, (h) cross-sectional schematic showing variable height of liquid pillars in adjacent unit cells, by controlling the air pressure selectively and (i) measured THz absorption with varying height of liquid pillars. Reproduced from [196]. CC BY 4.0.

the microfluidic metamaterial absorber showed strong THz absorption of over 90% with slight red shift in resonance frequency. The complementing features of microfluidic technology and THz metamaterials could potentially enable smart solutions by incorporating both sensing and reconfiguration modalities within a single device.

2.8. MEMS metadvice for THz detection

In all of the earlier mentioned approaches, an external stimulus drives the mechanical reconfiguration of MEMS actuators integrated with metasurface to achieve tunable THz response. Alternatively, incident THz waves can also drive the mechanical response of the MEMS actuators and hence employed for THz detection. MEMS metadvice based THz detector usually comprises of two parts—metamaterial absorber and sensing

element. The metamaterial absorber is a trilayer MIM configuration, where the bottom metal layer acts as the reflector, the central dielectric acts as the spacer and top metal layer is patterned to form the metamaterial. The MIM configuration is optimized to achieve high absorption at specific frequency. Based on the top metamaterial design advanced functionalities such as polarization selectivity and multispectral absorption can be readily realized [11, 197, 198]. Hence, the absorber converts the incident THz wave to heat and a sensing element is used to measure the rise in temperature. In one of the initial works, Au SRR metamaterial based absorbers were suspended with two bimaterial cantilevers made of Au/SiNx as shown in figure 10(a) [199]. The THz MEMS metadvice showed peak absorption at ~ 0.7 THz and led to the heating of the suspended SRR unit cells. The rise in temperature caused the mechanical bending of the suspended SRR unit cells. A

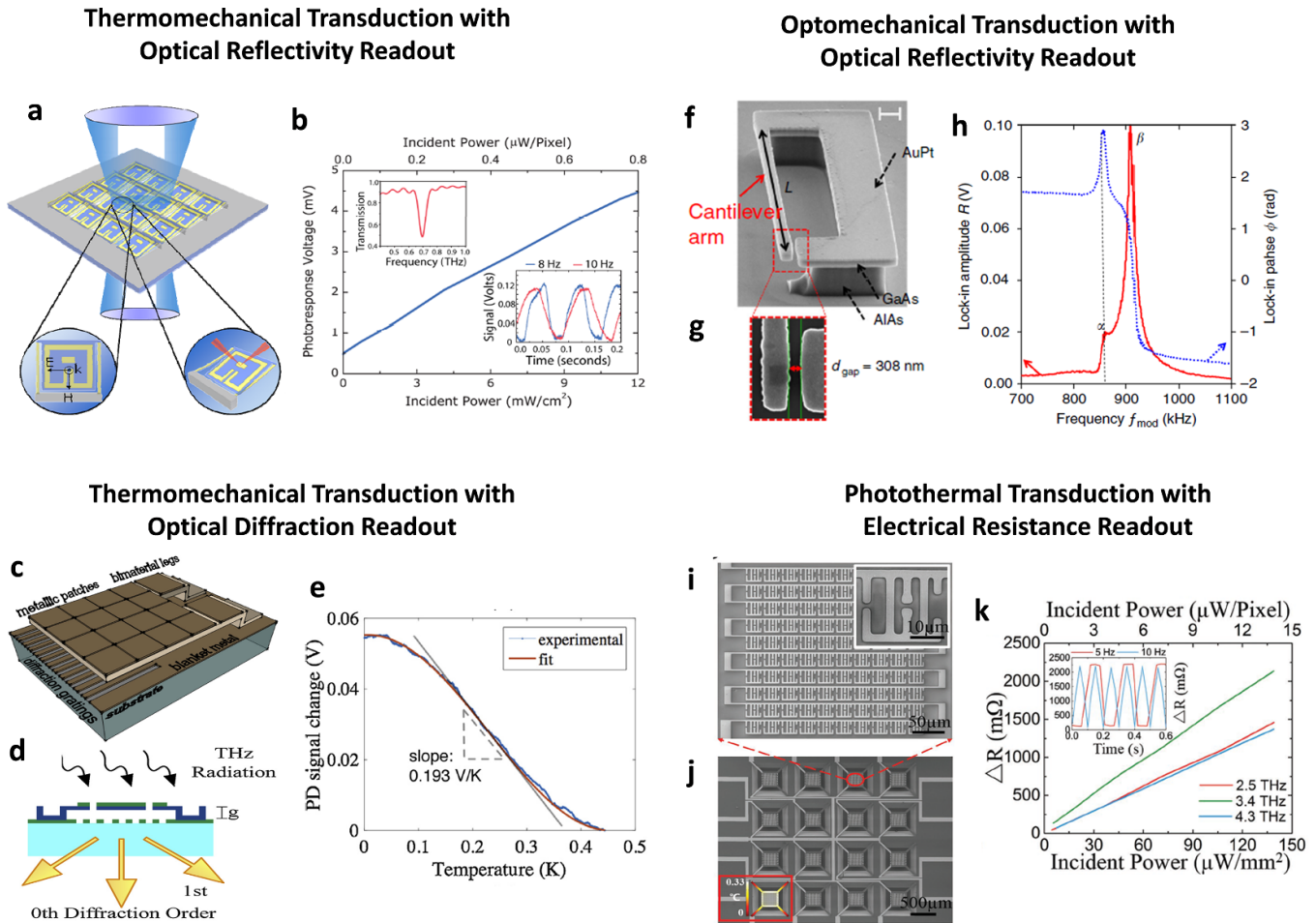


Figure 10. MEMS integrated metadevices for THz detection. (a) Schematic representation of the THz MEMS metadvice which deflects due to heating from THz absorption and the mechanical deflection is readout by optical beam reflection, (b) measured photoresponse voltage with respect to incident power with top-left inset showing peak absorption at ~ 0.7 THz and the bottom-right inset showing the temporal response of the sensor. Reprinted with permission from [199] © The Optical Society. (c) Schematic representation of the THz MEMS metadvice with suspended metamaterial layer with ground plane patterned as diffraction grating, (d) schematic representation showing the thermomechanical transduction and optical diffraction-based readout, (e) measured photodiode signal change with respect to temperature rise of the THz sensor. Reprinted from [204], Copyright (2016), with permission from Elsevier. (f) SEM image of the fabricated single metaatom optomechanical THz sensor, (g) zoomed in SEM image of the deeply subwavelength gap in the resonator, (h) measured lock-in amplitude and phase showing dual resonance in response to incident THz waves. Reproduced from [205] CC BY 4.0. (i) SEM image of the THz bolometer pixel with metamaterial absorber unit cell shown in the inset, (j) SEM image of the THz focal plane array with the thermal distribution simulation shown in the inset in the bottom-left, (k) measured change in electrical resistance with incident THz power at different frequencies. Reproduced from [208]. CC BY 4.0.

small metallic patch was fabricated within the SRR unit cell, which was used to reflect optical readout beam incident on the SRR unit cells. Based on the mechanical deformation, the position of the reflected optical beam varied and was calibrated for the incident THz power as shown in figure 10(b). The optical reflection based readout method provides improved sensitivity of THz detection. A highly optimized design was reported using the similar approach with Al/SiO₂ bimaterial cantilevers suspended THz absorber [200–202]. In this case, the bottom metal layer of the absorber was also used for reflection of the optical readout beam. However, this demands for etching away of Si substrate to allow for optical readout from the backside of the device. Alternatively, Al/SiNx bimaterial cantilever suspended metamaterial absorber was fabricated on glass substrate to allow for THz sensing from the front

size, while optical reflection was readout from the backside. The transparency of glass substrate to optical beams eliminates the need for etching thick substrates. A large array of 128×128 unit cells of MEMS metadvice was demonstrated for THz imaging application [203]. In another report, the thermomechanical deformation of parylene-C/Titanium bimaterial cantilever suspended THz absorber was measured using diffraction grating interferometer fabricated on the metal layer coated on substrate, below the suspended absorber as shown in figures 10(c)–(e) [204]. However, in the aforementioned MEMS metadvice based THz detectors, the response time is generally slow owing to the need for transfer of thermal energy and conversion to mechanical deformation. An innovative approach was reported by using a single SRR metaatom with a suspended cantilever as THz detector. The SRR metaatom

was designed to resonate at specific THz frequency and the suspended cantilever has a narrow in-plane gap of ~ 300 nm as shown in figures 10(f) and (g) [205]. The incident THz wave induce high-frequency currents and charges that, in turn, couple to the mechanical degrees of freedom as shown in figure 10(h). The mechanical reconfiguration of the suspended cantilevers was read out optically. This device had extremely small footprint, fast (>10 MHz) response time and potentially frequency-independent noise equivalent power. Even though thermomechanical transduction with optical readout provides higher sensitivity, it demands for complex calibration circuit to compensate the fabrication-related non-uniformity across the pixels as well as the requires precise alignment for optical readout. A more conventional approach of using bolometric detection has also been reported through integration of metamaterial absorber with MEMS bolometer as shown in figures 10(i) and (j) [206–208]. The metamaterial layer resonantly absorbs the incident THz wave and increases the temperature of the metadvice and this in turn leads to the corresponding rise in electrical resistance of the metallic line connecting the metamaterial unit cells, determined by the temperature coefficient of resistance of the metal. The change in resistance is then read out electrically as shown in figure 10(k). The bolometer pixels are released from the substrate to ensure efficient heat transfer and enhance the sensitivity of the detector. The advanced functionalities of metamaterial combined with the high sensitivity of MEMS detectors will play an key role in the development of next-generation miniaturized and low-cost THz imagers and spectrometers [209].

3. Future outlooks

The burgeoning field of THz technologies is gaining immense research momentum, due to its potential use in 6G communications, ultrasensitive biosensing, food quality inspection and low energy imaging for security screening. Metamaterials have provided an efficient means of achieving versatile THz manipulation. The integration of metamaterial with the robust and versatile platform of MEMS will translate these demonstrations to device level solutions for potential commercialization of THz technologies. So far, the focus had been to develop THz MEMS metadvice for single functionality such as frequency tunability, modulation, polarization control, tunable absorption, chirality switching and reconfigurable delay lines. The future evolution of THz MEMS metadvice is expected to be multidirectional. Research progress made so far in the field of THz MEMS metadvice will continue to progress, focussed on improved performance and addressing the limitations of current implementations in terms of switching speed, operational power and reliability. Research direction on exploring novel reconfiguration schemes, such as piezoelectric actuation, phase transition powered THz metadvice will also be a major thrust in the near future. Simultaneously, system level demonstration of THz metadvice by integrating control circuits and MEMS packaging will become essential for translation to commercial production [210]. Our perspective on some of the future research developments in the field of THz MEMS metadvice are discussed in this session.

3.1. Phase-transition powered reconfiguration

Large out-of-plane deformation to form reconfigurable 3D microstructures for THz MEMS metadvice have been reported either through annealing or pneumatic actuation [109, 159]. Both of these approaches require bulky systems for reconfiguration and are not attractive for commercial solutions. Alternatively, electrically reconfigurable out-of-plane deformation in THz MEMS metadvice are limited to small out-of-plane deformation [112, 118]. Recently, phase transition materials such as vanadium dioxide (VO_2) have been reported to achieve huge deformation with displacement to length ratio of ~ 1 , as shown in figure 11(a) [211–214]. Interestingly, the phase transition can be triggered using electrothermal stimulus and could enable highly integrated solution for realizing dynamic switching of metamaterial between planar and 3D configuration. Such large reconfiguration is essential for various applications, including chirality switching, widely tunable filters and absorbers. The range of deformation and transition temperature could also be varied either by doping or strain engineering of VO_2 [215]. Additionally, the memory effect in VO_2 can also be exploited for realizing THz memory metadvice with well-defined multilevel states, compared to the earlier reports [42]. Furthermore, the large strain built in the VO_2 layer will also ensure higher reliability of MEMS switches as it prevents stiction, which is one of the most common failure mechanism in electrostatic cantilever devices [216]. The availability of wide range of phase transition materials with unique properties could potentially enable novel functionalities in THz MEMS metadvice [214]. Currently, the experimental demonstration of VO_2 based THz MEMS metadvice is lacking, majorly due to the complexity in the fabrication, requiring large area devices. However, this challenge can be readily addressed and whole new sub-field of phase-transition powered THz MEMS metadvice can entail.

3.2. Three-dimensional reconfiguration

The wide variety of MEMS actuators with unique features can be co-designed and integrated with THz metamaterial to enable reconfiguration in all three spatial dimensions. An envisioned 3D reconfigurable metamaterial design is schematically shown in figure 11(b). It consists of two sets of comb-drive actuators for 2D planar reconfiguration, while the cantilevers integrated on the movable frame can enable out-of-plane reconfiguration. Hence, generic metamaterials can be fabricated and can be reconfigured based on the specific needs of various applications. This will be instrumental in driving down the cost of manufacturing, thereby making it an attractive solution for a wide range of THz applications.

3.3. Programmable reconfiguration

Programmable metamaterial is a device in which each unit cell can be addressed individually. This enables a single metadvice to be programmed to achieve various functionalities such as beam steering, holographic beam forming, and spatial light modulation [217]. Hence, programmable metamaterials

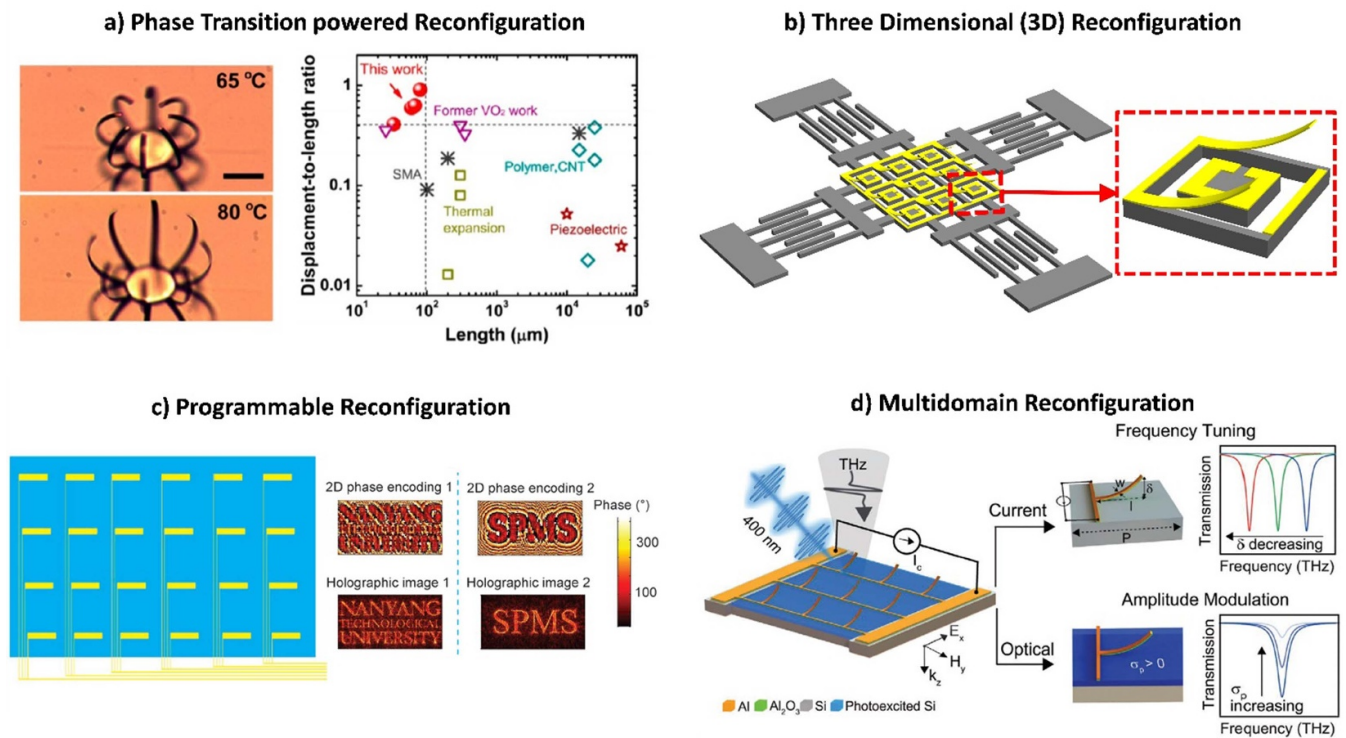


Figure 11. Future research directions for THz MEMS metadevices. (a) Phase transition powered cantilevers have the potential to enable dynamic switching between planar 2D and 3D configurations of THz metadevices and could provide novel functionalities. Reprinted with permission from [212]. Copyright (2012) American Chemical Society. (b) Schematics of THz MEMS metadvice that can be reconfigured in all three spatial dimensions by integrating comb drive actuators for 2D planar reconfiguration and cantilever approach for out-of-plane reconfiguration. (c) Programmable reconfiguration can be realized by isolating the control to unit cell level and will enable versatile functionalities of holographic beam forming, dynamic beam steering, polarization control and spatial light modulation. [127] John Wiley & Sons. © 2016 WILEY-VCH Verlag GmbH & Co. KGaA, Weinheim. (d) Multidomain reconfiguration showing the integration of MEMS with complementary reconfiguration schemes such as ultrafast optical control for advanced manipulation of THz waves. A multifunctional metamaterial showing spectral tuning with MEMS reconfiguration and ultrafast amplitude modulation due to photoexcitation of ion-irradiated Si substrate is also shown. [112] John Wiley & Sons. © 2020 WILEY-VCH Verlag GmbH & Co. KGaA, Weinheim.

are also known as software controlled metamaterials or reconfigurable intelligent surfaces. Programmable THz metamaterials are critical for the realization of holographic beam forming, dynamic beam steering and information metasurfaces in 6G communication links [104]. However, currently MEMS approach is limited to dual control, at best. Alternate solutions for higher level of control in active materials based THz metadevices, have been reported using VO₂ [45], liquid crystals [51, 53], high electron mobility transistor [29, 33, 218, 219], graphene [59, 220] and photoconductive semiconductor [221, 222]. These approaches are limited to line-wise or sub-array level control with compromised performance either in terms of phase contrast, speed or power consumption. Recently, NMOS transistor integrated THz programmable metasurface was reported for high speed and multifunctional operations [35]. However, the inherent limitation of operational frequency of NMOS transistor shows low switching contrast at 0.3 THz and hinders its scalability to even higher frequencies in the future. MEMS technology can provide an efficient solution with significantly larger switching contrast and lower power consumption. Simulation studies as shown in figure 11(c) validates the potential use of MEMS for the realization of THz programmable metamaterials [127]. However,

the complexity in fabrication, integration and characterization has hindered its experimental demonstration. Experimental realization of MEMS programmable THz metasurface will be an important research direction, owing to its relevance in 6G communications and integrated sensing applications [6, 35, 107].

3.4. Multidomain reconfiguration

Multidomain reconfiguration is critical for the realization of metamaterials with multiple functionalities and is gaining significant research attention, recently [39, 47, 183, 217]. Integration of MEMS with alternate approaches to alleviate the limitation of either of the approaches will be a major research direction in the future. Recently, the long-standing issue of narrowband operation of metamaterial integrated ultrafast THz modulators was addressed by integrating MEMS cantilever on ion-irradiated Si substrate as shown in figure 11(d) [112]. The electrothermal actuation of cantilevers enabled the operational frequency to be continuously tuned over the large spectral range of 0.3 THz, while the ion-irradiation of Si substrate enabled ultrafast modulation of THz resonance in picosecond timescales. Such integration of complementing

Table 1. Performance comparison of various MEMS actuators for enabling THz MEMS metadevices.

MEMS actuator	Deformation range	Operational speed	Reconfiguration direction	Range of reconfiguration	Power consumption	Footprint	Electrical control	CMOS compatibility
Thermal bimorph	Large	Slow (>ms)	Bidirectional	Full range	High	Low	No	Yes
Electrothermal bimorph	Large	Slow (>ms)	Unidirectional	Full range	High	Low	Yes	Yes
Electrothermal unimorph	Large	Slow (>ms)	Unidirectional	Full range	High	High	Yes	Yes
Electrostatic cantilever	Medium	Fast (> μ s)	Unidirectional	Limited range (Pull-in instability)	Low	Low	Yes	Yes
Electrostatic comb-drive	Large	Slow (>ms)	Bidirectional	Full range	Low	High	Yes	Yes
Electroactive polymer	Medium	Slow (>ms)	Bidirectional	Full range	Low	High	Yes	No
Pneumatic cantilevers	Large	Slow (>ms)	Bidirectional	Full range	High	High	No	No
Piezoelectric cantilevers	Medium	Fast (> μ s)	Bidirectional	Full range	Low	Low	Yes	Yes
Electromagnetic cantilevers	Large	Slow (>ms)	Bidirectional	Full range	High	High	Yes	No
Mechanically flexible	Large	Slow (>ms)	Bidirectional	Full range	High	High	No	No
Microfluidics	Large	Slow (> s)	Bidirectional	Full range	High	High	No	No
Phase transition bimorph	Large	Slow (>ms)	Unidirectional	Limited range (phase transition)	High	Low	Yes	No

technologies will become more attractive as they enable multifunctional feature within a single device.

4. Conclusions

The nascent field of THz metamaterials is rapidly growing due to its huge potential in various disruptive applications including - 6G wireless communications, non-destructive bio-sensing and imaging for security screening. The demand for technological translation of THz metamaterial into commercial solutions is becoming more crucial. The matured field of MEMS technology with its wide array of actuator designs and enhanced performance provides the perfect reconfiguration platform for large scale, miniaturized, low cost realization of THz devices. The wide range of MEMS actuators and their performance specifications are summarized in table 1. The variety of MEMS actuator designs and potential integration with complementing technologies for advanced metamaterial reconfiguration will play an important role in realizing multifunctional and programmable THz metadevices in the near future.

Data availability statement

No new data were created or analysed in this study.

Acknowledgments

The authors are grateful for the research funding of AME Programmatic Grant No. (A18A5b0056) from Agency for Science, Technology and Research (A*STAR), Singapore.

ORCID iDs

Prakash Pitchappa  <https://orcid.org/0000-0002-6168-4130>
 Ranjan Singh  <https://orcid.org/0000-0001-8068-7428>
 Chengkuo Lee  <https://orcid.org/0000-0002-8886-3649>
 Nan Wang  <https://orcid.org/0000-0003-1285-7530>

References

- [1] Siegel P H 2002 *IEEE Trans. Microw. Theory Tech.* **50** 3
- [2] Ferguson B and Zhang X-C 2002 *Nat. Mater.* **1** 1
- [3] Tonouchi M 2007 *Nat. Photon.* **1** 2
- [4] Nagatsuma T, Ducournau G and Renaud C C 2016 *Nat. Photon.* **10** 6
- [5] Withayachumnankul W, Fujita M and Nagatsuma T 2018 *Adv. Opt. Mater.* **6** 16
- [6] Sengupta K, Nagatsuma T and Mittleman D M 2018 *Nat. Electron.* **1** 12
- [7] Yang Y *et al* 2020 *Nat. Photon.* **14** 446–51
- [8] Aghasi H, Naghavi S M H, Tavakoli Taba M, Aseeri M A, Cathelin A and Afshari E 2020 *Appl. Phys. Rev.* **7** 2
- [9] Osborne I S 2008 *Science* **320** 5881
- [10] Yen T J *et al* 2004 *Science* **303** 5663
- [11] Tao H *et al* 2008 *Opt. Express* **16** 10
- [12] Withayachumnankul W and Abbott D 2009 *IEEE Photon. J.* **1** 2
- [13] Singh R *et al* 2009 *Phys. Rev. B* **79** 8
- [14] Singh R *et al* 2010 *Opt. Express* **18** 13
- [15] Singh R, Al-Naib I A I, Koch M and Zhang W 2011 *Opt. Express* **19** 7
- [16] Cong L *et al* 2015 *Adv. Opt. Mater.* **3** 11
- [17] Cong L, Xu N, Han J, Zhang W and Singh R 2015 *Adv. Mater.* **27** 42
- [18] Gupta M *et al* 2016 *Adv. Mater.* **28** 37
- [19] Cong L and Singh R 2019 *Adv. Opt. Mater.* **7** 13
- [20] Han S *et al* 2019 *Adv. Mater.* **31** 37
- [21] Lim W X *et al* 2018 *Adv. Opt. Mater.* **6** 19
- [22] Padilla W J, Taylor A J, Highstrete C, Lee M and Averitt R D 2006 *Phys. Rev. Lett.* **96** 10
- [23] Chen H-T, Padilla W J, Zide J M O, Gossard A C, Taylor A J and Averitt R D 2006 *Nature* **444** 7119
- [24] Chen H-T, O'Hara J F, Azad A K, Taylor A J, Averitt R D, Shrekenhamer D B and Padilla W J 2008 *Nat. Photon.* **2** 5
- [25] Chen H-T *et al* 2009 *Nat. Photon.* **3** 3
- [26] Shrekenhamer D, Rout S, Strikwerda A C, Bingham C, Averitt R D, Sonkusale S and Padilla W J 2011 *Opt. Express* **19** 10
- [27] Gu J *et al* 2012 *Nat. Commun.* **3** 1151
- [28] Zhang S *et al* 2012 *Nat. Commun.* **3** 942
- [29] Rout S and Sonkusale S R 2016 *APL Photonics* **1** 8
- [30] Manjappa M *et al* 2017 *Adv. Mater.* **29** 3
- [31] Lim W X *et al* 2018 *Adv. Mater.* **30** 9
- [32] Kumar A *et al* 2018 *Adv. Opt. Mater.* **6** 15
- [33] Zhao Y *et al* 2019 *Nano Lett.* **19** 11
- [34] Liu Y *et al* 2021 *J. Phys. D: Appl. Phys.* **54** 8
- [35] Venkatesh S, Lu X, Saeidi H and Sengupta K 2020 *Nat. Electron.* **3** 12
- [36] Burrow J A, Yahiaoui R, Sarangan A, Agha I, Mathews J and Searles T A 2017 *Opt. Express* **25** 26
- [37] Yahiaoui R, Burrow J A, Mekonen S M, Sarangan A, Mathews J, Agha I and Searles T A 2018 *Phys. Rev. B* **97** 15
- [38] Kodama C H and Coutu R A 2016 *Appl. Phys. Lett.* **108** 23
- [39] Pitchappa P, Kumar A, Prakash S, Jani H, Venkatesan T and Singh R 2019 *Adv. Mater.* **31** 12
- [40] Jeong Y-G, Bahk Y-M and Kim D-S 2020 *Adv. Opt. Mater.* **8** 3
- [41] Pitchappa P *et al* 2021 *Adv. Funct. Mater.* **31** 17
- [42] Driscoll T, Kim H-T, Chae B-G, Kim B-J, Lee Y-W, Jokerst N M, Palit S, Smith D R, Di Ventra M and Basov D N 2009 *Science* **325** 5947
- [43] Seo M *et al* 2010 *Nano Lett.* **10** 6
- [44] Wang D *et al* 2015 *Sci. Rep.* **5** 15020
- [45] Hashemi M R M, Yang S-H, Wang T, Sepúlveda N and Jarrahi M 2016 *Sci. Rep.* **6** 35439
- [46] Liu H, Lu J and Wang X R 2017 *Nanotechnology* **29** 024002
- [47] Shabanpour J, Beyraghi S and Cheldavi A 2020 *Sci. Rep.* **10** 8950
- [48] Yahiaoui R, Chase Z A, Kyaw C, Seabron E, Mathews J and Searles T A 2021 *J. Phys. D: Appl. Phys.* **54** 235101
- [49] Shrekenhamer D, Chen W-C and Padilla W J 2013 *Phys. Rev. Lett.* **110** 17
- [50] Liu Z *et al* 2013 *Opt. Express* **21** 5
- [51] Savo S, Shrekenhamer D and Padilla W J 2014 *Adv. Opt. Mater.* **2** 3
- [52] Shen Z-X *et al* 2019 *Appl. Phys. Lett.* **114** 4
- [53] Wu J *et al* 2020 *Appl. Phys. Lett.* **116** 13
- [54] Ju L *et al* 2011 *Nat. Nanotechnol.* **6** 10
- [55] Lee S H *et al* 2012 *Nat. Mater.* **11** 936–41
- [56] Lee S H *et al* 2013 *Sci. Rep.* **3** 2135
- [57] Srivastava Y K, Chaturvedi A, Manjappa M, Kumar A, Dayal G, Kloc C and Singh R 2017 *Adv. Opt. Mater.* **5** 23
- [58] Shi J *et al* 2018 *J. Mater. Chem. C* **6** 1291–306

- [59] Hosseinienejad S E, Rouhi K, Neshat M, Cabellos-Aparicio A, Abadal S and Alarcon E 2019 *IEEE Trans. Nanotechnol.* **18** 734–46
- [60] Ji J *et al* 2019 *Nanoscale* **11** 9429–35
- [61] Chanana A, Lotfizadeh N, Condori Quispe H O, Gopalan P, Winger J R, Blair S, Nahata A, Deshpande V V, Scarpulla M A and Sensale-Rodriguez B 2019 *ACS Nano* **13** 4
- [62] Gopalan P and Sensale-Rodriguez B 2020 *Adv. Opt. Mater.* **8** 3
- [63] Deinert J-C *et al* 2021 *ACS Nano* **15** 1
- [64] Mittendorf M, Winnerl S and Murphy T E 2020 *Adv. Opt. Mater.* **9** 2001500
- [65] Hu Y *et al* 2020 *Nano Energy* **68** 104280
- [66] Dai Z *et al* 2021 *ACS Appl. Mater. Sci.* **31** 2011011
- [67] Hu Y *et al* 2021 *ACS Photonics* **8** 3
- [68] Manjappa M *et al* 2017 *Adv. Mater.* **29** 32
- [69] Cong L, Srivastava Y K, Solanki A, Sum T C and Singh R 2017 *ACS Photonics* **4** 7
- [70] Chanana A, Zhai Y, Baniya S, Zhang C, Vardeny Z V and Nahata A 2017 *Nat. Commun.* **8** 1
- [71] Chanana A, Liu X, Zhang C, Vardeny Z V and Nahata A 2018 *Sci. Adv.* **4** 5
- [72] Manjappa M *et al* 2019 *Adv. Mater.* **31** 32
- [73] Kumar A *et al* 2020 *Sci. Adv.* **6** 8
- [74] Zhao D and Chia E E M 2020 *Adv. Opt. Mater.* **8** 3
- [75] Singh R, Lu J, Xie Z D, Yang J, Zhao G, Xu P, Qin Y Q and Zhu S N 2011 *Opt. Lett.* **36** 7
- [76] Xu W-Z, Marchetti L, Parlanti P, Landi S, Tonazzini I, Cecchini M, Piazza V and Gemmi M 2016 *Sci. Rep. Small* **12** 2610–615
- [77] Wu L *et al* 2017 *Sci. Rep.* **7** 6072
- [78] Wu L *et al* 2020 *ACS Appl. Electron. Mater.* **2** 8
- [79] Chen H-T *et al* 2010 *Phys. Rev. Lett.* **105** 24
- [80] Jin B *et al* 2010 *Opt. Express* **18** 16
- [81] Zhang C H *et al* 2012 *Appl. Phys. Lett.* **102** 081121
- [82] Singh R, Xiong J, Azad A K, Yang H, Trugman S A, Jia Q X, Taylor A J and Chen H-T 2012 *Nanophotonics* **1** 1
- [83] Grady N K *et al* 2013 *New J. Phys.* **15** 10
- [84] Srivastava Y K *et al* 2016 *Adv. Opt. Mater.* **4** 11
- [85] Srivastava Y K and Singh R 2017 *J. Appl. Phys.* **122** 18
- [86] Li C *et al* 2017 *Appl. Phys. Lett.* **111** 9
- [87] Wang D *et al* 2017 *Appl. Phys. Lett.* **110** 2
- [88] Srivastava Y K, Manjappa M, Cong L, Krishnamoorthy H N S, Savinov V, Pitchappa P and Singh R 2018 *Adv. Mater.* **30** 29
- [89] Keller J, Scalari G, Appugliese F, Mavrona E, Rajabali S, Süess M J, Beck M and Faist J 2018 *ACS Photonics* **5** 10
- [90] Bogue R 2013 *Sens. Rev.* **33** 4
- [91] Bogue R 2016 *Sens. Rev.* **36** 1
- [92] Mohd Ghazali F A, Hasan M N, Rehman T, Nafea M, Mohamed Ali M S and Takahata K 2020 *J. Micromech. Microeng.* **30** 7
- [93] Tao H *et al* 2008 MEMS and metamaterials: a perfect marriage at terahertz frequencies *IEEE Solid-State Sensor and Actuator Workshop (Hilton Head '08)* (Hilton Head Island, SC, USA)
- [94] Zhao X, Duan G, Li A, Chen C and Zhang X 2019 *Microsyst. Nanoeng.* **5** 1
- [95] Ren Z *et al* 2020 *Adv. Opt. Mater.* **8** 3
- [96] Yuhua C, Jingxuan W and Chengkuo L 2020 *Nanophotonics*
- [97] Guanxing Z *et al* 2021 *J. Opt.* **23** 1
- [98] Lin Y-S and Xu Z 2020 *Int. J. Optomechatron.* **14** 1
- [99] Demir K and Unlu M 2020 *J. Microelectromech. Syst.* **29** 4
- [100] Liu A Q *et al* 2012 *J. Opt.* **14** 11
- [101] Elayan H, Amin O, Shihada B, Shubair R M and Alouini M-S 2020 *IEEE Open J. Commun. Soc.* **1** 1–32
- [102] Ahmadivand A, Gerislioglu B, Ramezani Z, Kaushik A, Manickam P and Ghoreishi S A 2021 *Biosens. Bioelectron.* **177** 112971
- [103] Liaskos C, Nie S, Tsioliaridou A, Pitsillides A, Ioannidis S and Akyildiz I 2018 *IEEE Commun. Mag.* **56** 9
- [104] Cui T J, Liu S and Zhang L 2017 *J. Mater. Chem. C* **5** 3644–68
- [105] Tsilipakos O *et al* 2020 *Adv. Opt. Mater.* **8** 17
- [106] Fu X *et al* 2020 *Adv. Opt. Mater.* **8** 3
- [107] Wu X, Lu H and Sengupta K 2019 *Nat. Commun.* **10** 2722
- [108] Potekhina A and Wang C 2019 *Actuators* **8** 4
- [109] Tao H *et al* 2009 *Phys. Rev. Lett.* **103** 147401
- [110] Tao H, Strikwerda A C, Fan K, Padilla W J, Zhang X and Averitt R D 2011 *J. Infrared Millim. Terahertz Waves* **32** 5
- [111] Pitchappa P, Manjappa M, Krishnamoorthy H N S, Chang Y, Lee C and Singh R 2017 *Appl. Phys. Lett.* **111** 26
- [112] Pitchappa P, Kumar A, Liang H, Prakash S, Wang N, Bettiol A A, Venkatesan T, Lee C and Singh R 2020 *Adv. Opt. Mater.* **8** 12
- [113] Ho C P *et al* 2014 *Appl. Phys. Lett.* **104** 161104
- [114] Xu J *et al* 2020 *Opt. Express* **28** 7
- [115] Baracu A *et al* 2015 *AIP Conf. Proc.* **1646** 25
- [116] Lalas A, Kantartzis N and Tsiboukis T 2014 *Appl. Phys. A* **117** 2
- [117] Lalas A X, Kantartzis N V and Tsiboukis T D 2015 *Microsyst. Technol.* **21** 10
- [118] Pitchappa P, Ho C P, Dhakar L, Qian Y, Singh N and Lee C 2015 *J. Microelectromech. Syst.* **24** 3
- [119] Zhao X *et al* 2017 **970-3** 2017 *IEEE 30th Int. Conf. on Micro Electro Mechanical Systems (MEMS)*
- [120] Xu R and Lin Y S 2020 *J. Microelectromech. Syst.* **29** 5
- [121] Lin Y-S *et al* 2013 *Appl. Phys. Lett.* **102** 11
- [122] Ma F *et al* 2013 *Appl. Phys. Lett.* **102** 16
- [123] Ma F, Lin Y-S, Zhang X and Lee C 2014 *Light Sci. Appl.* **3** 5
- [124] Pitchappa P, Ho C P, Qian Y, Dhakar L, Singh N and Lee C 2015 *Sci. Rep.* **5** 11678
- [125] Zhao X *et al* 2018 *Optica* **5** 3
- [126] Cong L, Pitchappa P, Lee C and Singh R 2017 *Adv. Mater.* **29** 26
- [127] Cong L *et al* 2017 *Adv. Opt. Mater.* **5** 2
- [128] Hu F, Xu N, Wang W, Wang Y, Zhang W, Han J and Zhang W 2016 *J. Micromech. Microeng.* **26** 2
- [129] Pitchappa P *et al* 2015 Enhanced controllability in MEMS metamaterial **2015 28th IEEE Int. Conf. on Micro Electro Mechanical Systems (MEMS)** (<https://doi.org/10.1109/memsys.2015.7051138>)
- [130] Pitchappa P, Ho C P, Dhakar L and Lee C 2015 *Optica* **2** 6
- [131] Pitchappa P *et al* 2016 *Adv. Opt. Mater.* **4** 4
- [132] Manjappa M, Pitchappa P, Singh N, Wang N, Zheludev N I, Lee C and Singh R 2018 *Nat. Commun.* **9** 4056
- [133] Ho C P, Pitchappa P and Lee C 2016 *J. Appl. Phys.* **119** 15
- [134] Pitchappa P *et al* 2016 *Adv. Opt. Mater.* **4** 3
- [135] Cong L, Pitchappa P, Wang N and Singh R 2019 *Research* **2019** 1–11
- [136] Pitchappa P, Manjappa M, Ho C P, Singh R, Singh N and Lee C 2016 *Appl. Phys. Lett.* **109** 21
- [137] Shih K, Pitchappa P, Manjappa M, Ho C P, Singh R, Yang B, Singh N and Lee C 2017 *Appl. Phys. Lett.* **110** 16
- [138] Lin Y, Huang C and Lee C 2015 *IEEE J. Sel. Top. Quantum Electron.* **21** 4
- [139] Asgari S, Sharifi N and Granpayeh N 2019 *J. Micromech. Microeng.* **29** 4
- [140] Han Z *et al* 2014 *Opt. Express* **22** 18
- [141] Han Z *et al* 2015 *IEEE J. Sel. Top. Quantum Electron.* **21** 4
- [142] Tao H *et al* 2008 Dynamical control of terahertz metamaterial resonance response using bimaterial cantilevers *PIERS Proc.* (Cambridge, USA: The Electromagnetics Academy)
- [143] Unlu M *et al* 2014 *Sci. Rep.* **4** 5708
- [144] Unlu M and Jarrahi M 2014 *Opt. Express* **22** 26

- [145] Liu M *et al* 2017 *Microsyst. Nanoeng.* **3** 17033
- [146] Kan T *et al* 2013 *Appl. Phys. Lett.* **102** 22
- [147] Legtenberg R, Groeneveld A W and Elwenspoek M 1996 *J. Micromech. Microeng.* **6** 3
- [148] Fu Y H *et al* 2011 *Adv. Funct. Mater.* **21** 18
- [149] Zhu W M *et al* 2011 *Adv. Mater.* **23** 15
- [150] Zhu W M *et al* 2012 *Nat. Commun.* **3** 1274
- [151] Zhu W M *et al* 2011 *Appl. Phys. Lett.* **99** 22
- [152] Zhang M *et al* 2017 *Sci. Rep.* **7** 12068
- [153] Zhao X, Fan K, Zhang J, Keiser G R, Duan G, Averitt R D and Zhang X 2016 *Microsyst. Nanoeng.* **2** 16025
- [154] Ekmekci E, Strikwerda A C, Fan K, Keiser G, Zhang X, Turhan-Sayan G and Averitt R D 2011 *Phys. Rev. B* **83** 19
- [155] Huang Y *et al* 2020 *Sci. Rep.* **10** 20807
- [156] L alas A, Kantartzis N and Tsiboukis T 2014 *EPL* **107** 5
- [157] L alas A X, Kantartzis N V and Tsiboukis T D 2014 Reconfigurable terahertz metamaterials through piezoelectric microgrippers *9th IET Int. Conf. on Computation in Electromagnetics (CEM 2014)*
- [158] Matsui T, Inose Y, Powell D A and Shadrivov I V 2016 *Adv. Opt. Mater.* **4** 1
- [159] Kan T, Isozaki A, Kanda N, Nemoto N, Konishi K, Takahashi H, Kuwata-Gonokami M, Matsumoto K and Shimoyama I 2015 *Nat. Commun.* **6** 8422
- [160] Isozaki A, Kan T, Takahashi H, Matsumoto K and Shimoyama I 2015 *Opt. Express* **23** 20
- [161] Walia S, Shah C M, Gutruf P, Nili H, Chowdhury D R, Withayachumnankul W, Bhaskaran M and Sriram S 2015 *Appl. Phys. Rev.* **2** 1
- [162] Tao H *et al* 2008 *J. Phys. D: Appl. Phys.* **41** 23
- [163] Tao H *et al* 2008 *Phys. Rev. B* **78** 241103(R)
- [164] Cong L, Xu N, Gu J, Singh R, Han J and Zhang W 2014 *Laser Photon. Rev.* **8** 4
- [165] Srivastava Y K, Cong L and Singh R 2017 *Appl. Phys. Lett.* **111** 20
- [166] Woo J M, Kim D, Hussain S and Jang J-H 2014 *Opt. Express* **22** 3
- [167] Khodasevych I E *et al* 2010 Flexible fishnet metamaterial on PDMS substrate for THz frequencies *2010 Conf. on Optoelectronic and Microelectronic Materials and Devices*
- [168] Li J *et al* 2013 *Appl. Phys. Lett.* **102** 12
- [169] Li J *et al* 2013 *Opt. Lett.* **38** 12
- [170] Zhu M and Lee C 2015 *Opt. Mater. Express* **5** 4
- [171] Zhu M and Lee C 2015 *J. Lightwave Technol.* **33** 15
- [172] Liu X *et al* 2010 *Appl. Phys. Lett.* **96** 1
- [173] Zaichun C, Rahmani M, Yandong G, Chong C T and Minghui H 2012 *Adv. Mater.* **24** 23
- [174] Han N R *et al* 2011 *Opt. Express* **19** 8
- [175] Ortuño R, García-Meca C and Martínez A 2014 *Plasmonics* **9** 5
- [176] Khodasevych I E, Shah C M, Sriram S, Bhaskaran M, Withayachumnankul W, Ung B S Y, Lin H, Rowe W S T, Abbott D and Mitchell A 2012 *Appl. Phys. Lett.* **100** 6
- [177] Tao H *et al* 2010 *Adv. Mater.* **22** 32
- [178] Kim H S *et al* 2018 *Opt. Express* **26** 26
- [179] Sun L *et al* 2020 A degradable antibacterial skin patch of flexible terahertz metamaterials made from silk proteins *2020 IEEE 33rd Int. Conf. on Micro Electro Mechanical Systems (MEMS)*
- [180] Sun L *et al* 2020 *Small* **16** 17
- [181] Zhao X *et al* 2016 *J. Opt.* **18** 7
- [182] Lee S *et al* 2012 *Adv. Mater.* **24** 26
- [183] Morits D, Morits M, Ovchinnikov V, Omelyanovich M, Tamminen A, Tretyakov S and Simovski C 2014 *J. Opt.* **16** 3
- [184] Ako R T, Upadhyay A, Withayachumnankul W, Bhaskaran M and Sriram S 2020 *Adv. Opt. Mater.* **8** 3
- [185] Gupta B, Pandey S, Nahata A, Zhang T and Nahata A 2017 *Adv. Opt. Mater.* **5** 7
- [186] Shih K *et al* 2017 *J. Appl. Phys.* **121** 2
- [187] Geng Z *et al* 2017 *Sci. Rep.* **7** 16378
- [188] Shih K, Pitchappa P, Jin L, Chen C-H, Singh R and Lee C 2018 *Appl. Phys. Lett.* **113** 7
- [189] Seo M and Park H-R 2020 *Adv. Opt. Mater.* **8** 3
- [190] Shih K, Ren Z, Wang C and Lee C 2019 *J. Phys. D: Appl. Phys.* **52** 39
- [191] Zhang W *et al* 2018 *Adv. Phys. X* **3** 1
- [192] Zhang Z *et al* 2019 *Photon. Res.* **7** 12
- [193] Zhu W M *et al* 2014 Tunable meta-fluidic-materials base on multilayered microfluidic system *2014 IEEE 27th Int. Conf. on Micro Electro Mechanical Systems (MEMS)*
- [194] Wang J *et al* 2014 *Opt. Express* **22** 4
- [195] Song Q H *et al* 2016 Tunable metamaterials for terahertz ultra-broadband absorption driven by microfluidics *2016 IEEE 29th Int. Conf. on Micro Electro Mechanical Systems (MEMS)*
- [196] Song Q H *et al* 2017 *APL Mater.* **5** 6
- [197] Watts C M, Liu X and Padilla W J 2012 *Adv. Mater.* **24** 23
- [198] Brian T K *et al* 2013 *Opt. Eng.* **52** 1
- [199] Tao H *et al* 2011 *Opt. Express* **19** 22
- [200] Alves F, Grbovic D, Kearney B and Karunasiri G 2012 *Opt. Lett.* **37** 11
- [201] Alves F, Grbovic D, Kearney B, Lavrik N V and Karunasiri G 2013 *Opt. Express* **21** 11
- [202] Fabio A, Dragoslav G and Gamani K 2014 *Opt. Eng.* **53** 9
- [203] Wen Y *et al* 2017 *Microsyst. Nanoeng.* **3** 17071
- [204] Bilgin H, Zahertar S, Sadeghzadeh S, Yalcinkaya A D and Torun H 2016 *Sens. Actuators A* **244** 292–8
- [205] Belacel C, Todorov Y, Barbieri S, Gacemi D, Favero I and Sirtori C 2017 *Nat. Commun.* **8** 1578
- [206] Zhou Z *et al* 2017 A uncooled multi-band metamaterial detector focal plane array for real-time multi-spectral terahertz wave sensing and imaging *2017 IEEE 30th Int. Conf. on Micro Electro Mechanical Systems (MEMS)*
- [207] Zhou Z *et al* 2018 Metamaterials to see in terahertz in “colors” *2018 IEEE Micro Electro Mechanical Systems (MEMS)*
- [208] Zhou Z *et al* 2018 *Adv. Sci.* **5** 7
- [209] Sizov F 2018 *Semicond. Sci. Technol.* **33** 12
- [210] Xu J, Du Y, Tian Y and Wang C 2020 *Int. J. Optomechatron.* **14** 1
- [211] Rúa A, Fernández F E and Sepúlveda N 2010 *J. Appl. Phys.* **107** 7
- [212] Wang K *et al* 2013 *ACS Nano* **7** 3
- [213] Merced E, Tan X and Sepúlveda N 2013 *Sens. Actuators A* **196** 30–37
- [214] Ma H *et al* 2020 *J. Appl. Phys.* **128** 10
- [215] Shao Z, Cao X, Luo H and Jin P 2018 *NPG Asia Mater.* **10** 7
- [216] Dong K *et al* 2018 *Small* **14** 14
- [217] Tian H W, Shen H Y, Zhang X G, Li X, Jiang W X and Cui T J 2020 *Front. Phys.* **8** 448
- [218] Chan W L *et al* 2009 *Appl. Phys. Lett.* **94** 21
- [219] Karl N, Reichel K, Chen H-T, Taylor A J, Brenner I, Benz A, Reno J L, Mendis R and Mittleman D M 2014 *Appl. Phys. Lett.* **104** 9
- [220] Liu Y *et al* 2020 *Opt. Express* **28** 17
- [221] Cong L, Srivastava Y K, Zhang H, Zhang X, Han J and Singh R 2018 *Light Sci. Appl.* **7** 28
- [222] Cong L and Singh R 2020 *Adv. Mater.* **32** 28